Impact of gas-phase mechanisms on Weather Research Forecasting Model with Chemistry (WRF/Chem) predictions: Mechanism implementation and comparative evaluation

Yang Zhang,[1] Yaosheng Chen,[1] Golam Sarwar,[2] and Kenneth Schere[2]

Received 4 February 2011; revised 25 October 2011; accepted 26 October 2011; published 7 January 2012.

[1] Gas-phase mechanisms provide important oxidant and gaseous precursors for secondary aerosol formation. Different gas-phase mechanisms may lead to different predictions of gases, aerosols, and aerosol direct and indirect effects. In this study, WRF/Chem-MADRID simulations are conducted over the continental United States for July 2001, with three different gas-phase mechanisms, a default one (i.e., CBM-Z) and two newly implemented ones (i.e., CB05 and SAPRC-99). Simulation results are evaluated against available surface observations, satellite data, and reanalysis data. The model with these three gas-phase mechanisms gives similar predictions of most meteorological variables in terms of spatial distribution and statistics, but large differences exist in shortwave radiation and temperature and relative humidity at 2 m at individual sites under cloudy conditions, indicating the importance of aerosol semi-direct and indirect effects on these variables. Large biases exist in the simulated wind speed at 10 m, cloud water path, cloud optical thickness, and precipitation, due to uncertainties in current cloud microphysics and surface layer parameterizations. Simulations with all three gas-phase mechanisms well reproduce surface concentrations of O_3, CO, NO_2, and $PM_{2.5}$, and column NO_2. Larger biases exist in the surface concentrations of nitrate and organic matter (OM) and in the spatial distribution of column CO, tropospheric ozone residual, and aerosol optical depth, due to uncertainties in primary OM emissions, limitations in model representations of chemical transport, and radiative processes. Different gas-phase mechanisms lead to different predictions of mass concentrations of O_3 (up to 5 ppb), $PM_{2.5}$ (up to 0.5 μg m^{-3}), secondary inorganic $PM_{2.5}$ species (up to 1.1 μg m^{-3}), organic PM (up to 1.8 μg m^{-3}), and number concentration of $PM_{2.5}$ (up to 2×10^4 cm^{-3}). Differences in aerosol mass and number concentrations further lead to sizeable differences in simulated cloud condensation nuclei (CCN) and cloud droplet number concentration (CDNC) due to the feedback mechanisms among H_2SO_4 vapor, $PM_{2.5}$ number, CCN, and CDNC through gas-phase chemistry, new particle formation via homogeneous nucleation, aerosol growth, and aerosol activation by cloud droplets. This study illustrates the important impact of gas-phase mechanisms on chemical and aerosol predictions, their subsequent effects on meteorological predictions, and a need for an accurate representation of such feedbacks through various atmospheric processes in the model. The online-coupled models that simulate feedbacks between meteorological variables and chemical species may provide more accurate representations of the real atmosphere for regulatory applications and can be applied to simulate chemistry-climate feedbacks over a longer period of time.

Citation: Zhang, Y., Y. Chen, G. Sarwar, and K. Schere (2012), Impact of gas-phase mechanisms on Weather Research Forecasting Model with Chemistry (WRF/Chem) predictions: Mechanism implementation and comparative evaluation, *J. Geophys. Res.*, *117*, D01301, doi:10.1029/2011JD015775.

1. Introduction

[2] Gas-phase mechanisms, which describe the chemistry of important oxidants and gaseous precursors for secondary air pollutants, such as ozone (O_3) and secondary aerosols, have been a critical component of air quality models (AQMs) since 1970s. Different gas-phase mechanisms may

[1]Department of Marine, Earth, and Atmospheric Sciences, North Carolina State University, Raleigh, North Carolina, USA.
[2]Atmospheric Modeling and Analysis Division, National Exposure Research Laboratory, U.S. Environmental Protection Agency, Research Triangle Park, North Carolina, USA.

0148-0227/12/2011JD015775

lead to different gaseous and aerosol predictions. Intercomparisons of gas-phase mechanisms with box and Lagrangian models have been extensively conducted under representative simple scenarios or atmospheric chemical regimes [e.g., *Hough*, 1988; *Derwent*, 1990, 1993; *Olson et al.*, 1997; *Kuhn et al.*, 1998; *Jimenez et al.*, 2003; *Chen et al.*, 2009; *Emmerson and Evans*, 2009]. These models, however, have their limitations and cannot accurately represent the real atmosphere. Such limitations can be overcome by using three-dimensional (3-D) AQMs, which have also been used commonly for mechanism comparisons [e.g., *Gross and Stockwell*, 2003; *Yarwood et al.*, 2003; *Faraji et al.*, 2008; *Luecken et al.*, 2008; *Sarwar et al.*, 2008, 2011; *Kim et al.*, 2009, 2011a, 2011b]. As reported in previous studies, the carbon-bond mechanism version IV (CBM-IV) of *Gery et al*. [1989] and the 2005 carbon bond mechanism (CB05) of *Yarwood et al.* [2005] give similar results in winter [*Sarwar et al.*, 2008]. Both CB05 and the Statewide Air Pollution Research Center Mechanism (SAPRC-99) of W. P. L. Carter (http://www.cert.ucr.edu/~carter/absts.htm#saprc99) give much higher O_3 than CBM-IV [*Yarwood et al.*, 2003; *Sarwar et al.*, 2008; *Luecken et al.*, 2008], and SAPRC-99 gives even higher O_3 than CB05 in summer [*Luecken et al.*, 2008]. The differences between CBM-IV and SAPRC-99 are attributed to more reaction products from oxidation of aromatics by hydroxyl radical (OH) and higher radical and aldehydes (>C6, ALDX) produced from SAPRC-99 [*Faraji et al.*, 2008], as well as different representations of cycling of nitrogen oxides (NO_x) and oxidized nitrogen compounds (NO_z), secondary products and their reactions under low-NO_x conditions, updated cross section and quantum yields for photolysis [*Luecken et al.*, 2008]. Differences between CB05 and SAPRC-99 are attributed primarily to more reactive aromatic fragments but lower amount of acetaldehyde (ALD2) in SAPRC-99 and differences in kinetic parameters for chemical reactions, such as the product coefficients of alkenes and secondary aldehydes [*Faraji et al.*, 2008; *Luecken et al.*, 2008]. CB05 and SAPRC-99 are more similar in spatial patterns than either one is with CBM-IV, due to their more consistent reactions and rates [*Luecken et al.*, 2008]. Differences among mechanisms are most likely to occur in areas with large biogenic volatile organic compounds (BVOCs) emissions due to their high reactivity [*Luecken et al.*, 2008]. All these intercomparisons focus on the impact on gaseous species, such as O_3, NO_x, and VOCs, except for *Sarwar et al*. [2008] and *Kim et al.* [2011a]. *Sarwar et al*. [2008] compared aerosol predictions with the same aerosol module but two gas-phase mechanisms, CB-IV and CB05. They found that results with both mechanisms gave similar secondary aerosol predictions under winter conditions but results with CB05 gives lower (by 2%–10%) secondary aerosol concentrations than CB-IV under summer conditions. *Kim et al*. [2011a] studied the impacts of two different gas-phase mechanisms (CB05 and Regional Atmospheric Chemical Mechanism, version 2 (RACM2), 2008, http://airquality.ucdavis.edu/pages/events/2008/acm/Goliff.pdf) on secondary aerosol formation over Europe in a 3-D AQM and found that differences in monthly-mean $PM_{2.5}$ concentrations are less than 1 $\mu g\ m^{-3}$ (6%), with up to 26% differences in $PM_{2.5}$ compositions. In addition, all these studies use offline-coupled meteorology-chemistry models that cannot account for interactions between meteorology and chemistry. An exception was *Arteta et al*. [2006] who applied an online coupled Regional Atmospheric Modeling Systems (RAMS) model with two different gas-phase mechanisms, but in that study no aerosol formation was simulated.

[3] In contrast to offline AQMs, online models can provide more realistic treatments of the atmosphere, particularly in regions with a fast local circulation or high aerosol loading and cloud coverage where meteorology and radiation may be modified by the presence of chemical species through various feedback mechanisms [*Grell et al.*, 2000; *Audiffren et al.*, 2004; *Minvielle et al.*, 2004; *Brulfert et al.*, 2005; *Zhang*, 2008]. These online coupled models have been applied for real-time air quality forecasting and studies of interactions between climate and air pollutants [e.g., *Grell et al.*, 2005; *Fast et al.*, 2006; *Zhang et al.*, 2010a, 2010b; *Chuang et al.*, 2011; *N. Zhang et al.*, 2011].

[4] In this study, three different gas-phase mechanisms are compared using an online 3-D AQM, the Weather Research and Forecasting Model with Chemistry (WRF/Chem) version 3.0 [*Grell et al.*, 2005; *Fast et al.*, 2006] with the Model of Aerosol, Dynamics, Reaction, Ionization, and Dissolution (MADRID) of *Zhang et al*. [2004, 2010a, 2010b] (referred to as WRF/Chem-MADRID). This comparison differs from previous studies by examining three commonly used gas-phase mechanisms in an online coupled meteorology-chemistry-aerosol-cloud-radiation system, i.e., WRF/Chem, and their impacts on gaseous and aerosol species and meteorological predictions, as well as the direct and indirect aerosol effects. The objectives are to (1) examine the impacts of different gas-phase mechanisms on WRF/Chem predictions of meteorological parameters, gases, aerosols, and aerosol direct and indirect effects; and (2) identify important sources of uncertainties in modeling meteorology, chemistry, and their interactions through various feedback mechanisms for future model improvements. Section 2 describes the modeling episode, configurations, and the gas-phase mechanisms used. In section 3, modeling results are compared and evaluated against available surface observations, satellite data, and reanalysis data. Impacts of gas-phase mechanisms on model predictions are examined. Important model uncertainties are assessed through comparative evaluation and mechanistic analysis. Major findings, challenges, and future studies are summarized in section 4.

2. Model Configurations and Simulation Design

2.1. Modeling Episode and Model Description

[5] WRF/Chem-MADRID simulations are conducted at a horizontal resolution of 36-km over the contiguous U.S. for July 2001. The model components and configurations used in this study are summarized in Table 1. Physical options are the same as those used by *Zhang et al.* [2010b], except for several updates in WRF/Chem version 3.0, including improvements of Monin-Obukhov surface layer scheme under zero wind conditions [*Monin and Obukhov*, 1954; *Janjić*, 2001], Yonsei University (YSU) planetary boundary layer (PBL) scheme under stable conditions [*Hong et al.*, 2006], Purdue Lin microphysics for graupel ventilation factor [*Lin et al.*, 1983; *Chen and Sun*, 2002], and the use of a positive definite advection scheme of *Skamarock and*

Table 1. Model Components and Configurations

Simulation Period	1–31 July 2001
Domain	Continental U.S.
Horizontal resolution	36 km
Vertical resolution	34 layers from 1000–100 mb, with 12 layers in PBL
Meteorological IC and BC	The National Centers for Environmental Predictions Final Analysis (NCEP-FNL) reanalysis data; re-initialization every 4 days
Shortwave radiation	Goddard shortwave radiation scheme [*Chou et al.*, 1998]
Longwave radiation	The rapid radiative transfer model (RRTM) [*Mlawer et al.*, 1997]
Land surface	Community National Centers for Environmental Prediction (NCEP), Oregon State University, Air Force, and Hydrologic Research Lab-NWS Land Surface Model (NOAH) [*Chen and Dudhia*, 2001; *Ek et al.*, 2003]
Surface layer	Monin-Obukhov [*Monin and Obukhov*, 1954; *Janjić*, 2001]
PBL	Yonsei University Scheme (YSU) [*Hong et al.*, 2006]
Cumulus	Grell-Devenyi ensemble [*Grell and Devenyi*, 2002]
Microphysics	Purdue Lin [*Lin et al.*, 1983; *Chen and Sun*, 2002]
Aerosol activation	Abdul-Razzak and Ghan (A-R & G) [*Abdul-Razzak and Ghan*, 2002]
Gas-phase chemistry	CBM-Z [*Zaveri and Peters*, 1999], CB05 [*Yarwood et al.*, 2005], and SAPRC-99 (http://www.cert.ucr.edu/∼carter/absts.htm#saprc99)
Photolysis	Fast-J [*Wild et al.*, 2000]
Aerosol module	Model of Aerosol, Dynamics, Reaction, Ionization, and Dissolution (MADRID) [*Zhang et al.*, 2004, 2010b]
Aqueous-phase chemistry	Carnegie Mellon University (CMU) mechanism of *Fahey and Pandis* [2001]
Chemical IC	Community Multiscale Air Quality (CMAQ) modeling system [*Binkowski and Roselle*, 2003; *Byun and Schere*, 2006]
Chemical BC	The Goddard Earth Observing System Atmospheric Chemistry Transport Model (GEOS-Chem) except for O_3, which is taken from the NCAR's Community Atmosphere Model (CAM)
Anthropogenic/biogenic emissions	The 1999 National Emissions Inventory (NEI) version 3
Sea-salt emissions	*Gong et al.* [2002]

Weisman [2009] that was not available in WRF/Chem v2.2 used in *Zhang et al*. [2010b]. Atmospheric processes considered include emissions, transport, diffusion, photolysis, gas- and aqueous-phase reactions, aerosol processes, aerosol-cloud interactions, dry deposition, and wet scavenging. Meteorological and chemical initial conditions (ICON) and boundary conditions (BCON) and anthropogenic/biogenic emissions are also the same as those in *Zhang et al.* [2010b], which demonstrated an overall satisfactory performance of WRF/Chem. While WRF/Chem offers options to use online BVOCs emissions, offline BVOCs emissions are used in this study. BVOCs emissions affect chemical predictions which affect feedbacks of chemical species to meteorology and the altered meteorology will in turn affect BVOCs emissions and chemical predictions during next time step, leading to different BVOC emissions, chemical predictions, and accumulated feedbacks to meteorology that can be attributed in part to different BVOCs emissions and in part to different gas-phase mechanisms. Using offline-generated fixed BVOCs emissions will enable an examination of the changes in predicted chemical concentrations due only to changes in gas-phase chemical mechanisms and subsequent changes in feedbacks to meteorology, rather than changes due to a combination of different gas-phase chemical mechanisms and different online BVOCs emissions.

[6] Two major aerosol-radiation feedbacks (i.e., the aerosol direct effect by scattering and absorbing solar radiation and indirect effect by acting as cloud condensation nuclei (CCN)) are considered in WRF/Chem 2.2 and newer versions [*Fast et al.*, 2006]. Several recent studies [e.g., *Fast et al.*, 2006; *Gustafson et al.*, 2007; *Zhang*, 2008; *Chapman et al.*, 2009; *Zhang et al.*, 2010b] have shown the importance of these aerosol direct and indirect effects on a regional scale using WRF/Chem with CBM-Z and the Model for Simulating Aerosol Interactions and Chemistry (MOSAIC) that does not treat the formation of secondary organic aerosol (SOA). *Zhang et al.* [2010a] incorporated the updated version of MADRID of *Zhang et al.* [2004] and *Pun et al.* [2005] into WRF/Chem version 3.0 and coupled it with an existing gas-phase mechanism (i.e., the Carbon Bond Mechanism-Z (CBM-Z) of *Zaveri and Peters* [1999]) and default modules for aerosol direct and indirect effects in WRF/Chem. Similar to MOSAIC, MADRID uses a sectional size representation. Eight size sections over 0.0215–10 μm with fixed size boundaries for each section are used to represent the aerosol size distribution. MADRID differs in many aspects of aerosol treatments from MOSAIC. For example, MADRID treats SOA formation from 25 condensable species using an absorptive approach. It simulates the homogeneous binary nucleation of sulfuric acid and water vapor following the approach of *McMurry and Friedlander* [1979], which accounts for the competition between nucleation and condensation. MADRID offers three options for simulating gas/particle mass transfer: bulk equilibrium, hybrid, and kinetic approaches. The bulk equilibrium is used in this work. When bulk equilibrium approach is used, condensation is implicitly treated by allocating the transferred mass to different size sections based on the condensational growth law. The growth of particles over sections due to various growth processes is simulated using the moving-center scheme of Jacobson [*Jacobson*, 2005], in which the size boundaries of each section are fixed but the diameter representative of the section is allowed to move within and across the boundaries according to the growth law. The coagulation between particles is simulated using the algorithm of *Jacobson et al.* [1994]. Different from many

aerosol models that only simulate PM mass concentrations and diagnose PM number concentrations from the simulated mass concentrations and assumed section representative diameters, MADRID uses the so-called two-moment method to explicitly simulate jointly for PM mass and number concentrations by accounting for their changes due to various atmospheric processes (e.g., emission, transport, nucleation, condensation, coagulation, cloud processing, and removal). The representative diameter for each section is calculated using simulated particle mass and number concentrations for receptive size section. A more detailed description of MADRID along with recent updates can be found in *Zhang et al.* [2004, 2010a, 2010c]. The initial application of WRF/Chem-MADRID for a 5 day episode over eastern Texas has shown reasonably good predictions of meteorological variables and surface concentrations and column mass of chemical species [*Zhang et al.*, 2010b]. WRF/Chem-MADRID has also been or is being applied to air quality backcasting in other regions in the U.S. and the continental United States (CONUS), Europe, China, and Mexico [e.g., *Y. Zhang et al.*, 2011; *Zhu and Zhang*, 2011] and forecasting in the southeastern United States [e.g., *Chuang et al.*, 2011; *N. Zhang et al.*, 2011].

[7] In this study, WRF/Chem-MADRID is further developed by implementing two gas-phase mechanisms, i.e., CB05 [*Yarwood et al.*, 2005] and SAPRC-99 (http://www.cert.ucr.edu/∼carter/absts.htm#saprc99), into WRF/Chem version 3.0 using the Kinetic PreProcessor (KPP) [*Salzmann*, 2007, 2008] and coupling them with MADRID. An interface is developed between gaseous concentrations predicted from three gas-phase mechanisms (i.e., CBM-Z, CB05, and SAPRC-99) and the Goddard shortwave as well as the Rapid Radiative Transfer Model (RRTM) longwave radiation schemes by accounting for changes in radiation due to simulated changes in mixing ratios of O_3 (instead of using the default O_3 profile). WRF/Chem-MADRID simulations with the three gas-phase mechanisms are conducted over CONUS for July 2001, a summer month during which differences in model predictions caused by different gas-phase mechanisms are potentially large. This episode was also simulated by *Zhang et al.* [2010b] using an older version of WRF/Chem (i.e., version 2.2) with CBM-Z and MOSAIC. Another important difference between this work and *Zhang et al.* [2010b] is that SOA is simulated in WRF/Chem-MADRID with CB05 and SAPRC-99 in this effort. The SOA formation was not included in previous WRF/Chem simulations with MOSAIC because CBM-Z was hard-wired with a numerical solver (instead of the generalized KPP) in WRF/Chem and SOA condensable precursors could not be directly added into it.

[8] As described in *Fast et al.* [2006], aerosol radiative properties in WRF/Chem are simulated based on the Mie theory, and aerosol direct radiative forcing is calculated using the Goddard shortwave radiative transfer model of *Chou et al.* [1998]. As described in *Chapman et al.* [2009], the aerosol indirect effects in WRF/Chem are simulated through aerosol-cloud-radiation-precipitation interactions. CCN spectrum is determined as a function of PM number concentrations and updraft velocity following the aerosol activation/resuspension parameterization of *Abdul-Razzak and Ghan* [2002] that is based on the Kőhler theory. Cloud droplet number concentrations (CDNC) are then predicted from first principles by accounting for their changes due to major atmospheric processes including droplet nucleation/aerosol activation, advection of droplets from adjacent grid cells droplet loss from evaporation, collision/coalescence, collection by rain, ice, and snow, and freezing to form ice crystals following the parameterization of *Ghan et al.* [1997], which has been added to the existing Lin microphysics scheme [*Lin et al.*, 1983; *Chen and Sun*, 2002] to allow the two-moment treatment of cloud water (cloud water mass and cloud droplet number) in WRF/Chem. As indicated by *Ghan et al.* [1997], the number of droplet nucleated depends primarily on PM number concentration and updraft velocity, as well as the PM composition and size distribution. The cloud-precipitation interactions are simulated by accounting for the dependence of autoconversion of cloud droplets to rain droplets on CDNC based on the parameterization of *Liu et al.* [2005]. The cloud-radiation interactions are simulated by linking simulated CDNC with the Goddard shortwave radiation scheme and the *Lin et al.* microphysics scheme [*Skamarock et al.*, 2005].

[9] CBM-Z and CB05 are two variants of CBM-IV of *Gery et al.* [1989], a condensed mechanism that has been primarily developed based on the lumped structure method for urban studies. CBM-Z is designed to extend the CBM-IV framework to regional and global scale applications [*Zaveri and Peters*, 1999]. CB05 is designed to better simulate biogenics, toxics, PM formation, and acid deposition under pristine, wintertime, and high altitude conditions [*Yarwood et al.*, 2005]. Compared with CBM-IV, CBM-Z and CB05 include some up-to-date kinetic data, additional nitric acid and organic nitrate reactions, explicitly treated methane, ethane, and methylperoxy radicals, and added lumped species such as alkenes with internal double bonds and higher organic peroxides. CB05 includes one more hydrogen reaction, a few more odd-oxygen reactions, NO_3 radical reactions, and NO_x recycling reactions, which may be important under very dry conditions in upper troposphere, pristine conditions, nighttime conditions, and very cold conditions, respectively [*Sarwar et al.*, 2008]. CBM-Z has more detailed isoprene chemistry than CB05, but CB05 includes terpene chemistry that is not treated in CBM-Z. Compared with CBM-Z, CB05 does not treat acetone, but treats lumped species including ALDX and its corresponding peroxyacyl radicals, peroxynitrites, carboxylic acids, and peroxycarboxylic acids. *Whitten et al.* [2010] recently revised CB05 to incorporate updated toluene chemistry (i.e., CB05-TU). According to *Sarwar et al.* [2011], CB05-TU increases monthly 8 h O_3 by 1–3 ppb (2%–5%) in some urban areas in the U.S. and has a small impact (mostly <1%) on $PM_{2.5}$ concentrations. The use of CB05-TU is not expected to change air pollution control strategy that is based on CB05. Unlike CBM-Z and CB05, SAPRC-99 is a condensed mechanism that is based on the lumped species method. Compared with CB05, SAPRC-99 is similar to other mechanisms in its representation of reactions of isoprene, terpene, and ALDX, but more detailed in categorizing peroxy radicals, peroxyacytyl nitrate (PAN) analogues, isoprene products, organic acids, and alkanes. SAPRC-99 also treats more chemical species including acetone, ketones, and aromatic aldehydes (http://www.cert.ucr.edu/∼carter/absts.htm#saprc99). Many reaction rate constants are different in SAPRC-99 and CB05. SAPRC07 [*Carter*, 2010], an

updated version of SAPRC-99, is expected to give predictions closer to CB05 [*Luecken et al.*, 2008]. Relative to the detailed mechanism of SAPRC-99, the averaged maximum incremental reactivity values and simulated maximum O_3 levels due to updates in SAPRC07 decrease by ~10% and up to 7%, respectively [*Carter*, 2010].

[10] Similar to *Zhang et al.* [2010a, 2010b], SOA is not included in the simulation of WRF/Chem-MADRID with CBM-Z in this work, because of the limitation in the implementation of CBM-Z in WRF/Chem mentioned previously. However, SOA is treated in the WRF/Chem-MADRID simulations with CB05 and SAPRC-99 using a new SOA module that simulates 25 SOA species formed by absorbing oxidation products of biogenic VOCs including isoprene and terpene and anthropogenic VOCs including toluene, xylene, higher molecular alkane, and polycyclic aromatic hydrocarbon. In this SOA module, terpene has been split into sesquiterpene and five monoterpene families including surrogate species for α-pinene and sabinene, surrogate species for β-pinene and Δ3-carene, limonene, terpinene, and surrogate species for other monoterpenes, with speciation factors of 7.4%, 24.8%, 29.4%, 16.4%, 0.6%, and 21.3%, respectively [*Seinfeld and Pankow*, 2003; *Kanakidou et al.*, 2005]. Additional reactions are added into CB05 and SAPRC-99 to produce 25 SOA precursors for the SOA module in MADRID. One main difference between SAPRC-99 and CB05 is that SAPRC-99 produces SOA from high molecular alkane, whereas CB05 does not, because high molecular alkane is not included in the lumped structure approach used in CB05.

2.2. Model Evaluation Protocols and Databases

[11] Model evaluation is performed using an evaluation protocol that follows *Zhang et al.* [2006a] and *Office of Air Quality Planning and Standards* (*OAQPS*) [2007]. The simulated meteorological variables, chemical concentrations, and aerosol and cloud properties are evaluated against available surface observations, satellite data, and reanalysis data. The evaluation protocol includes spatial distribution, temporal variation, column abundances, and overall statistical metrics. The statistical measures used here include the normalized mean bias (NMB) and the normalized mean gross error (NME) (see their definitions in *Zhang et al.* [2006a]). Simulation results within the relaxation zones (defined as the five grid cells closest to each lateral boundary) are excluded in the statistics calculation to eliminate unreliable predictions of cloud properties and radiative fluxes caused by specified lateral boundary conditions. Detailed temporal (hourly) variations of meteorological and chemical predictions are analyzed at 8 sites (Jefferson Street (JST), Atlanta, Ga.; Yorkville (YRK), Ga.; North Birmingham (BHM), Ala.; Centreville (CTR), Ala.; Gulfport (GFP), Miss.; Oak Grove (OAK), Miss.; Pensacola (PNS), Fla.; and Outlying Landing Field (OLF), Fla.) from the Southeastern Aerosol Research and Characterization Study Experiment (SEARCH).

[12] Tables 2 and 3 summarize observational networks and variables, measurement methods, and associated accuracies/uncertainties included in the model evaluation. Surface networks include the Clean Air Status and Trends Network (CASTNET, http://www.epa.gov/castnet/), the Speciation Trend Network (STN, http://www.epa.gov/ttn/amtic/speciepg.html), the Air Quality System (AQS, http://www.epa.gov/ttn/airs/airsaqs/), the Interagency Monitoring of Protected Visual Environments (IMPROVE, http://vista.cira.colostate.edu/improve/), SEARCH (http://www.atmospheric-research.com/studies/SEARCH), and the National Atmospheric Deposition Program (NADP, http://nadp.sws.uiuc.edu). CASTNET provides data to assess trends in air quality, atmospheric deposition, and ecological effects due to changes in air pollutant emissions. It contains continuous meteorological measurements (e.g., surface incoming shortwave radiation (SWD), surface pressure (P), 2 m temperature (T2), 2 m relative humidity (RH2), wind speed and direction at 10 m (WSP10 and WDR10), continuous O_3 measurements), as well as weekly samples for sulfate (SO_4^{2-}), nitrate (NO_3^-), ammonium (NH_4^+), sulfur dioxide (SO_2), and nitric acid (HNO_3) at 83 sites across the United States. Most sites are located in rural or remote locations where the influence of pollutant emissions is minimal. STN was designed to monitor and gather data on the chemical composition of fine particles to characterize annual and seasonal spatial distributions and trends of $PM_{2.5}$. It contains 24 h average (every 3 days) measurements of $PM_{2.5}$, SO_4^{2-}, NO_3^-, NH_4^+, EC, and OC at 54 sites in urban areas. IMPROVE was established to document long-term trends for assessing progress towards the national visibility goal and monitor regional haze in support of the State Implementation Plan for Regional Haze in Class I areas (e.g., national parks and wilderness areas). It provides 24 h average samples for $PM_{2.5}$, SO_4^{2-}, NO_3^-, NH_4^+, EC, and OC for every third day (midnight to midnight, local time) at 134 sites in the United States. AQS was established as a repository of the ambient air quality data collected by the U.S. Environmental Protection Agency (EPA), state, local, and tribal air pollution control agencies from thousands of monitoring stations. It provides ambient concentrations of criteria and hazardous air pollutants at monitoring sites, primarily in cities and towns in the United States. For example, hourly O_3 measurements are available at 1161 sites for July 2001. SEARCH was established to address regulatory and scientific questions on O_3 and its precursors, PM mass and composition, mercury speciation and deposition, wet deposition of acidity and nutrients, and atmospheric visibility. It provides hourly meteorological and chemical (e.g., P, T2, RH2, WSP10, and WDR10, nitrogen dioxide (NO_2), nitric oxide (NO), carbon monoxide (CO), reactive nitrogen compounds (NO_y), SO_2, HNO_3, O_3, $PM_{2.5}$, and $PM_{2.5}$ compositions) measurements and 24 h average measurements of $PM_{2.5}$ and $PM_{2.5}$ compositions at 8 sites that are grouped into pairs of urban/rural or urban/suburban sites located in the southeastern United States. NADP was designed to record long-term data on the amounts, trends, and geographic distributions of acids, nutrients, and base cations in precipitation, as well as weekly total measurements of precipitation over 250 sites in the United States.

[13] The observational datasets include meteorological variables (e.g., SWD, P, T2, RH2, WSP10, WDR10, U10, V10, weekly and daily Precip, and chemical concentrations (e.g., hourly gaseous concentrations including O_3, SO_2, HNO_3, and 24 h averaged aerosol concentrations including $PM_{2.5}$, sulfate (SO_4^{2-}), nitrate (NO_3^-), ammonium (NH_4^+), black carbon (BC), organic carbon (OC), and organic matters (OM)). Wind is evaluated using wind speed and its

Table 2. Measurement Methods and Associated Accuracy or Uncertainty for Meteorological and Radiative Variables From Various Networks

Network	Parameter[a]	Method	Accuracy[b]	Reference
CASTNET	SWD	Pyranometer	±10%	*CASTNET* [2005]
	T2	Platinum Resistance temperature detectors	±0.5°C	*CASTNET* [2005]
	RH2	Thin Film Capacitor	±5% for RH >85%, ±20% for RH <85%	*CASTNET* [2005]
	WSP10	Anemometer	The greater of ±0.5 m s^{-1} for wind speed <5 m s^{-1} or ±5% for wind speed ≥5 m s^{-1}	*CASTNET* [2005]
	WDR10	Wind Vane	±5 °	*CASTNET* [2005]
STN	P	Commercial speciation sampler's sensor	±10 mmHg	*OAQPS* [2000]
	T2	Commercial speciation sampler's sensor	±2 °C	*OAQPS* [2000]
NADP	Precip	Rain gauges	±0.03 in. (or 1%) for weighting gauges; 1% at rain rate of 1 in. h^{-1}, 4% at 3 in. h^{-1}, and up to 6% at 6 in. h^{-1} for tip bucket gauge	*EPA* [1983]
CMAP	Precip	Observations from rain gauges are merged with precipitation estimates from satellite-based algorithms (infrared and microwave)	5%–10% for global average; larger uncertainties for individual grid area values	*Xie and Arkin* [1997]
SEARCH	SWD	Pyranometer	10 w m^{-2}	*Desert Research Institute* (*DRI*) [2002a]
	P	A barometric pressure sensor	1 mb	*DRI* [2002a]
	T2	Thermistor or platinum resistance thermometer	±0.4°C	*DRI* [2002a]
	RH2	Capacitive relative humidity device	±5%	*DRI* [2002a]
	WSP10	Wind speed sensor	±1.5% or ±0.11 m s^{-1}	*DRI* [2002a]
	WDR10	Wind direction sensor	±5°	*DRI* [2002a]
NOAA-CDC	OLR	NOAA Polar-orbiting satellite measurements with temporal and spatial interpolation	N/A	*Liebmann and Smith* [1996]
MODIS	PWV	The MODIS near-IR water vapor retrieval algorithm	5%–10% (uncertainty)	*Gao and Kaufman* [2003]
	CWP	Retrieval technique using visible/near infrared sensor (0.4–14.4 μm) with 36 channels (MODIS/SEVIRI)	15 ∼ 25 g m^{-2} (Random error)	*Bennartz* [2007] *Seethala* [2011]
	CF	Calculated based on cloud reflectance derived from MODIS cloud mask or cloud optical property retrieval	10% (Random error)	*Bennartz* [2007]; *Pincus et al.* [2011]
	COT	Retrieved by minimizing the difference between the observed intensity in one visible and one near-infrared wavelength	8%(Random error) 13% (Mean error)	*Bennartz* [2007] *Janssen et al.* [2011]
	AOD	MODIS aerosol retrieval algorithms	±0.05 ± 0.15τ over land and ±0.03 ± 0.05τ over the ocean (uncertainty); Bias < +0.2 for 80% of data	*Remer et al.* [2005] *Hyer et al.* [2010]
	CCN	Calculated based on MODIS aerosol size distribution retrieval	N/A	*Remer et al.* [2005]
	CDNC	Estimated based on MODIS cloud property retrieval	<80% when CF >0.8 and CWP >25 g/m^2 (uncertainty)	*Bennartz* [2007]

[a]SWD, surface incoming shortwave radiation; OLR, outgoing longwave radiation; P, pressure; T2, temperature at 2 m; RH2, relative humidity at 2 m; WSP10, wind speed at 10 m; WDR10, wind direction at 10 m; U10, U component of WSP10; V10, V component of WSP10; Precip, precipitation; PWV, precipitable water vapor; CWP, cloud water path; CF, cloud fraction; COT, cloud optical thickness; AOD, aerosol optical depth; CCN, cloud condensation nuclei; CDNC, cloud droplet number concentration; SEVIRI, Spinning Enhanced Visible and InfraRed Imager.
[b]Values are accuracy unless otherwise noted.

west-east and south-north components, i.e., U and V, respectively. OC observations by IMPROVE and SEARCH are converted to OM by multiplying by 1.4 for comparison with model predictions of OM, despite some uncertainties associated with this value [*White and Roberts*, 1977; *Turpin and Lim*, 2001]. BC and OC observations by STN are combined to obtain total carbon (TC) for comparisons with simulated TC because STN uses the thermo-optical transmittance protocol that is different from thermo-optical reflectance protocol used by the SEARCH and IMPROVE networks. The uncertainties and/or biases associated with these measurements due to various possible sources of errors in instruments and/or measurement methods are summarized in Tables 2 and 3.

[14] Satellite data include outgoing longwave radiation (OLR) from the National Oceanic and Atmospheric Administration Climate Diagnostic Center (NOAA-CDC), tropospheric ozone residual (TOR) from the Total Ozone Mapping Spectrometer/Solar Backscattered Ultra Violet (TOMS/SBUV), column NO_2 from the Global Ozone Mapping Experiment (GOME), column CO from the Measurements of Pollution in the Troposphere (MOPITT), precipitable water vapor (PWV), cloud water path (CWP), cloud fraction (CF), cloud optical depths (COT), aerosol optical depth (AOD), and CCN from the Moderate Resolution Imaging Spectroradiometer (MODIS), and CDNC in warm cloud derived by *Bennartz* [2007] using MODIS data. Terra orbits cross the equator at 10:30 local time. To

Table 3. Measurement Methods and Associated Accuracies or Uncertainties or Errors for Chemical Variables From Various Networks

Network	Parameter	Method[a]	Accuracy	Reference
CASTNET	O_3	UV absorbance	±10%	*CASTNET* [2005]
	SO_4^{2-}	IC	±5%	*CASTNET* [2005]
	NO_3^-	IC	±5%	*CASTNET* [2005]
	NH_4^+	AC	±10%	*CASTNET* [2005]
AQS	O_3	UV absorbance	±2%	*OAQPS* [2008]
IMPROVE	$PM_{2.5}$	The Aerosol Sampler with Teflon filter, gravimetric PIXE/PESA XRF Absorption	±5 μg	*OAQPS* [2002]
	SO_4^{2-}	IC	±5%	*OAQPS* [2002]
	NO_3^-	IC	±5%	*OAQPS* [2002]
	NH_4^+	IC	±5%	*OAQPS* [2002]
	BC	TOR Carbon Combustion Analysis	±5%	*OAQPS* [2002]
	OC	TOR Carbon Combustion Analysis	±5%	*OAQPS* [2002]
STN	$PM_{2.5}$	Commercial speciation sampler's flow rate sensor with Teflon filter	±10%	*OAQPS* [1999]
	SO_4^{2-}	IC	10%[b]	*OAQPS* [1999]
	NO_3^-	IC	10%[b]	*OAQPS* [1999]
	NH_4^+	IC	10%[b]	*OAQPS* [1999]
	BC	TOR Carbon Combustion Analysis	15%[b]	*OAQPS* [1999]
	OC	Same as above	15%[b]	*OAQPS* [1999]
SEARCH	O_3	Ultraviolet absorption (TEIOA, Model 49)	±1%	*DRI* [2002b]
	CO	Nondispersive infrared spectroscopy	±1% or −0.5 ± 12.1%	*DRI* [2002c], *Hansen et al.* [2003]; *Edwards et al.* [2004]
	SO_2	UV-fluorescence	±1%	*DRI* [2002c], *Hansen et al.* [2003]
	HNO_3	Denuder diff./Mo reduction/chemiluminescence	±1%	Same as above
	NO_2	Photolysis/chemiluminescence	±1%	Same as above
	NO	Chemiluminescence	±1%	Same as above
	$PM_{2.5}$	TEOM for hourly and FRM with Teflon filters	±2%	*DRI* [2002d], *Hansen et al.* [2003]
	SO_4^{2-}	Fe reduction/UV-fluorescence for hourly and PCM(CH1) particle composition monitor, channel 1	±1%	*DRI* [2002e], *Hansen et al.* [2003], *SEARCH* [2003]
	NO_3^-	Filter diff./Mo reduction/chemiluminescence for hourly and PCM(CH1) particle composition monitor, channel 1	±1%	Same as above
	NH_4^+	Filter diff./Pt oxidation/chemiluminescence for hourly and PCM(CH1) particle composition monitor, channel 1	±1%	Same as above
	BC	Oxidative combustion (R&P 5400) for hourly and PCM(CH3) particle composition monitor, channel 3	±2%	*DRI* [2002f], *Hansen et al.* [2003]
	OC	Same as above	±2%	*DRI* [2002f], *Hansen et al.* [2003]
TOMS/SBUV	TOR	The Earth Probe Total Ozone Mapping Spectrometer	±3% for the absolute error and ±2% for the random error	*McPeters et al.* [1998]
MOPITT	CO	Gas-correlation radiometry	±10% for accuracy, and 20%–30% for RMSE	*Emmons et al.* [2007], *Deeter et al.* [2009]
GOME	NO_2	The GOME UV/visibility spectrometer	1.5×10^{15} cm^{-2} (or 35%–60%) under highly-polluted conditions	*Boersma et al.* [2004]

[a]IC, ion chromatography; AC, automated colorimetry; TOR, thermal optical reflectance; TEIOA, thermo environmental instruments ozone analyzers; TEOM, tapered element oscillating microbalance; PCM (CH1), particle composition monitor, channel; R&P, Rupprecht & Patashnick; RMSE, root mean squire error.

[b]The values are the measurement quality objective for total measurement error expressed as coefficient of variation.

evaluate all observations related to MODIS, the monthly-mean AODs from WRF/Chem are calculated as an average of values during 1500–2000 UTC when the Terra satellite passes over the continental United States, following *Roy et al.* [2007]. CWP is calculated as the summation of cloud water as liquid, ice, rain, snow, and graupel [*Otkin and Greenwald*, 2008]. CDNC in warm cloud is calculated as an average value within the layer of 150∼800 m from the ground during cloudy periods. Reanalysis data include precipitation from the Climate Prediction Center (CPC) Merged Analysis of Precipitation (CMAP), in which observations from rain gauges are merged with precipitation estimates from several satellite-based algorithms (infrared and microwave) to produce pentad (5 day) and monthly analyses of precipitation [*Xie and Arkin*, 1997]. All satellite data and reanalysis data are re-gridded to the simulation domain for model evaluation. Similar to surface observations, uncertainties and/or biases associated with satellite data and retrieval algorithms as summarized in Tables 2 and 3 could help explain some differences between simulation results and observations.

3. Results and Discussions

3.1. Meteorological Variables

[15] Table 4 summarizes performance statistics of the meteorological predictions from the simulations with three gas-phase mechanisms. Figures 1 and 2 show spatial distributions of simulated monthly-mean meteorological variables compared against observations from surface networks and satellite data and reanalysis data. Only results from WRF/Chem-MADRID simulation with CB05 are shown because all WRF/Chem-MADRID simulations with different gas-phase mechanisms give overall similar monthly-mean spatial distribution of predicted meteorological variables

Table 4. Performance Statistics for Meteorological and Radiative Predictions[a]

Variable	Data Source	Data Point	Mean Obs.	Mean Sim.			NMB (%)			NME (%)		
				CBM-Z	CB05	SAPRC-99	CBM-Z	CB05	SAPRC-99	CBM-Z	CB05	SAPRC-99
SWD (hourly, W m^{-2})	CASTNET	45381	312.2	379.9	383.0	381.1	21.7	22.7	22.1	38.5	38.5	38.6
	SEARCH	5776	224.8	260.7	263.6	258.2	16.0	17.3	14.9	50	47	49.2
SWD (max, W m^{-2})	CASTNET	2333	826.2	951.4	954.8	953.1	15.2	15.6	15.4	19.5	19.5	19.3
	SEARCH	245	777.4	915.5	919.4	907.8	17.8	18.3	16.8	24.8	23.7	23.9
OLR (W m^{-2})	NOAA-CDC	14076	250.0	243.8	243.5	243.6	−2.5	−2.6	−2.6	6.1	6.1	6.1
P (hPa)	STN	992	991.8	984.6	984.5	984.5	−0.7	−0.7	−0.7	1	1	1
	SEARCH	5655	1002.5	1000.9	1000.8	1000.9	−0.2	−0.2	−0.2	0.4	0.4	0.4
T2 (°C)	CASTNET	55415	21.0	21.6	21.6	21.6	2.8	2.9	2.9	12.5	12.5	12.5
	STN	993	25.2	24.2	24.2	24.2	−3.9	−3.8	−3.8	8	8	8.1
	SEARCH	5682	27.6	27.8	27.8	27.8	0.5	0.6	0.4	7.9	8	8
RH2 (%)	CASTNET	55658	67.2	63.8	63.7	63.8	−5.1	−5.2	−5.1	17.6	17.6	17.6
	SEARCH	5677	80.5	68.4	68.5	68.5	−15.0	−14.9	−14.9	17.2	17.2	17.1
WSP10 (m s^{-1})	CASTNET	55857	2.0	3.9	3.9	3.9	97.6	98.4	98.3	113	113.7	113.6
	SEARCH	5624	1.8	2.7	2.73	2.7	49.0	50.4	50.0	77.6	78.9	77.8
WDR10 (°)	CASTNET	55844	188.6	199.7	199.6	199.6	5.9	5.9	5.8	40.1	40.2	40.1
	SEARCH	5814	189.4	199.7	199.6	199.1	5.5	5.4	5.2	43.3	42.8	43.3
U10 (m s^{-1})	CASTNET	55781	0.3	1.1	1.1	1.1	307.9	306.8	304.6	810.6	812.8	814.6
	SEARCH	5624	0.2	1.0	1.0	1.0	372.6	373.6	370.4	755	749.1	751.3
V10 (m s^{-1})	CASTNET	55855	0.3	0.4	0.4	0.4	14.6	13.8	14.1	621.7	626	623
	SEARCH	5624	0.1	0.3	0.3	0.3	153.0	157.4	133.1	1243.4	1262	1257
Precip. (mm wk^{-1})	NADP	768	20.7	31.7	31.9	31.9	53.0	54.0	54.2	112.7	114.8	114.1
Precip. (mm day^{-1})	CMAP	14076	2.4	3.6	3.7	3.7	53.4	55.6	54.6	85.7	87.4	86.5
PWV (cm)	MODIS	14076	3.4	3.0	3.0	3.0	−11.5	−11.5	−11.5	11.7	11.8	11.8
CWP (g m^{-2})	MODIS	14076	182.3	58.8	59.3	59.0	−67.7	−67.4	−67.6	71.8	71.9	72.0
CF (%)	MODIS	14076	56.2	53.1	53.1	53.1	−5.6	−5.6	−5.6	21.4	21.6	21.5
COT	MODIS	14076	16.0	4.1	3.8	3.9	−74.7	−76.4	−75.8	−74.7	−76.5	−75.8
AOD	MODIS	14058	0.2	0.2	0.2	0.2	2.5	5.0	7.2	50.2	45.3	47.8
CCN (cm^{-2})	MODIS	5776	0.43×10^9	1.57×10^9	1.20×10^9	1.55×10^9	263.1	178.7	258.4	263.1	178.7	258.4
CDNC (cm^{-3})	*Bennartz* [2007]	7950	217.6	137.4	114.4	126.0	−36.9	−47.4	−42.1	60.5	62.2	61.3

[a]SWD, surface incoming shortwave radiation; OLR, outgoing longwave radiation; P, pressure; T2, temperature at 2 m; RH2, relative humidity at 2 m; WSP10, wind speed at 10 m; WDR10, wind direction at 10 m; U10, U component of WSP10; V10, V component of WSP10; Precip, precipitation; PWV, precipitable water vapor; CWP, cloud water path; CF, cloud fraction; COT, cloud optical thickness; AOD, aerosol optical depth; CCN, cloud condensation nuclei; CDNC, cloud droplet number concentration.

including SWD, OLR, P, T2, RH2, WSP10, WDR10, Precip, PWV, CWP, CF, and COT, despite differences in their magnitudes at specific locations (see section 3.3). Among them, the differences in simulated COT are the largest with domain-wide mean percentage difference of <5% between simulations. The monthly mean meteorological predictions of WRF/Chem version 3.0 in this study are also similar to those of version 2.2 in *Zhang et al.* [2010a].

[16] Simulated OLR is comparable with NOAA-CDC observations in terms of spatial distributions and magnitude (Figure 1), with NMBs of −2.6% to −2.5% (Table 4). Overpredictions of OLR by >10 W m^{-2} are found over most states in the Midwest and northeastern United States, where CF is underpredicted. Underpredictions of OLR by >10 W m^{-2} are found over the southeastern and northwestern coastal areas, where CF is overpredicted. The opposite trends of OLR and CF in those areas demonstrate clearly the role of clouds in trapping the outgoing infrared radiation emitted by the Earth's surface. A reliable parameterization is not yet available to account for the contribution of convective clouds to cloud water content. As a result, CWP is significantly underestimated over most of the domain with an NMB of −67.4%, although the magnitude of CF is more comparable with the MODIS observations with an NMB of −5.6%. CWP is overpredicted over the Atlantic Ocean and the coastal areas, which coincides with significant overpredictions of CF and Precip. COT is significantly underpredicted over the entire domain, with NMBs of −76.4% to −74.7%, due not only to underpredicted CWP but also to the fact that COTs considered here are only from water and ice. COTs from rain, snow, and graupel are not accounted for. While large differences exist in the simulated versus observed spatial distributions of CWP, COT, and CF, simulated and observed PWV are overall consistent in terms of both magnitudes and spatial distributions. The CMAP reanalysis data give comparable precipitation to NADP surface observations, but its horizontal resolution of 2.5° × 2.5° is not fine enough to capture the considerable spatial variability, especially over the eastern U.S. where heavy precipitation was observed by NADP but is significantly underestimated by the CMAP reanalysis data. Comparing with the CMAP reanalysis data, the simulation better captures spatial variability of NADP observed precipitation, but significantly overpredicts precipitation intensity with NMBs of 53.0%–54.2% against NADP and 53.4%–55.6% against CMAP, which is attributed to too frequent afternoon convective rainfall and/or an overestimation in the amount of the rainfall simulated by the Grell-Devenyi ensemble cumulus parameterization in summer. The overprediction of precipitation coincides with the underprediction of PWV and CWP over most of the domain, showing uncertainties in simulated atmospheric water budget. The uncertainties in PWV, CWP, and precipitation directly affect aerosol thermodynamics, aqueous-phase chemistry, and wet scavenging, respectively.

[17] Comparisons with observations indicate that SWD is overestimated over the entire domain (Figure 2), with NMBs

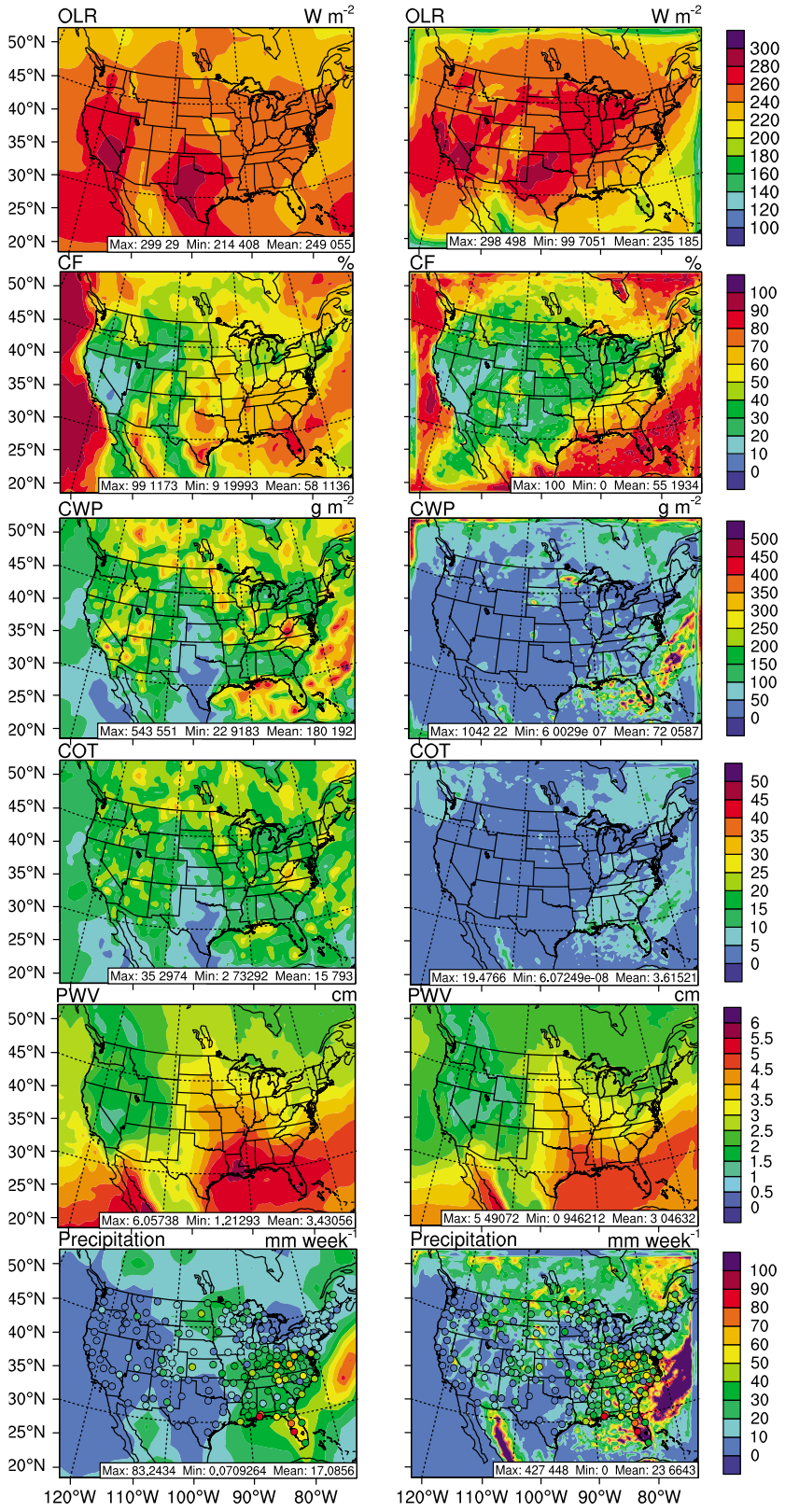

Figure 1. Spatial distributions of meteorological variables in comparison with satellite data or re-analysis data. From the first to sixth rows: OLR, outgoing longwave radiation; CF, cloud fraction; CWP, cloud water path; COT, cloud optical depth; PWV, precipitable water vapor; and precipitation from satellite data including NOAA-CDC (OLR) and MODIS (CF, CWP, COT, and PWV), and CMAP reanalysis data and NADP data (indicated by circles (Precip, left)), and WRF/Chem-MADRID simulations with CB05 and overlay with NADP data for Precip (right). The observational data are indicated by circles.

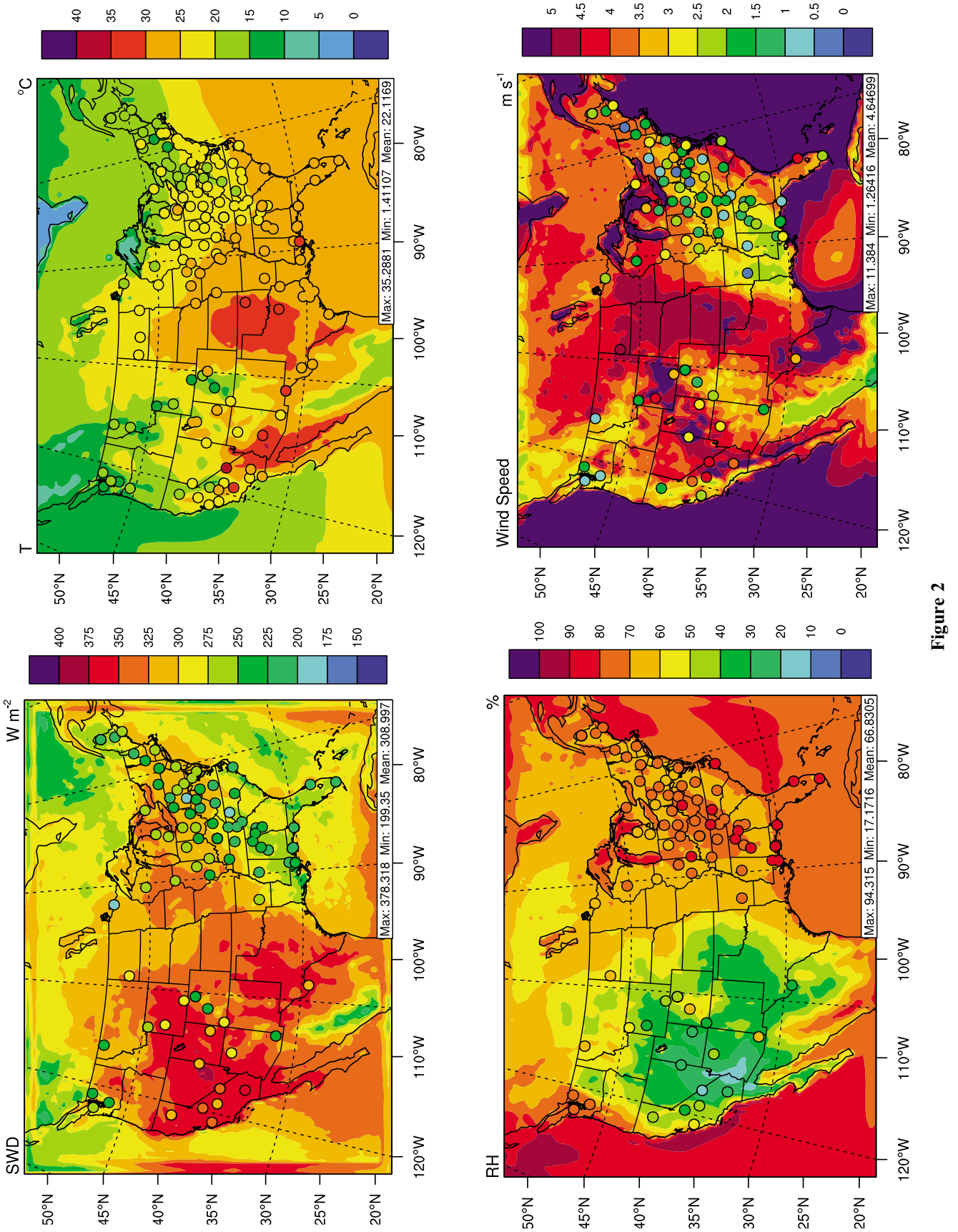
T
°C
Max: 35.2881 Min: 1.41107 Mean: 22.1169
Wind Speed
m s-1
Max: 11.384 Min: 1.26416 Mean: 4.64699
SWD
W m-2
Max: 378.318 Min: 199.35 Mean: 308.997
RH
%
Max: 94.315 Min: 17.1716 Mean: 66.8305
50°N
45°N
40°N
35°N
30°N
25°N
20°N
120°W
110°W
100°W
90°W
80°W

Figure 2

of 14.9%–22.7% for hourly values and 15.2%–15.6% for daily maximum value (Table 4). Similar overpredictions in SWD were also reported in *Otte* [2008a]. Since current models are able to well reproduce shortwave radiative transfer under clear sky conditions [*Chou and Suarez*, 1999; *Li and Trishchenko*, 2001; *Tarasova et al.*, 2006; *Miao et al.*, 2008], the overprediction of surface shortwave radiation may be likely due to uncertainties associated with cloud radiative forcing. Despite uncertainties in the predictions of radiative variables, surface P and T2 are well reproduced, except for a few observational sites. Some studies [e.g., *Tarasova et al.*, 2006; *Zhang et al.*, 2010a] have shown that with the Monin-Obukhov surface layer parameterization and NOAH land surface model, a monthly-mean difference in SWD up to 80 W m^{-2} (equivalent to an NMB above 20%) would not induce a difference in T2 greater than 1°C (equivalent to an NMB about 5%). However, using the NOAH land surface model tends to give a dry bias for near-surface RH (with an overall NMB of −15.0% to −5.1%) due to excessive latent heat fluxes [*Sanjay*, 2008], since WSP10 is significantly overpredicted in the entire domain with NMBs of 49.0%–98.4% (as shown in Table 4 and Figure 2). The similarity theory used by Monin-Obukhov surface layer parameterization scheme could induce large uncertainties in deriving vertical wind profiles, especially under stable conditions. This is supported by the fact that the differences between simulated and observed WSP10 are found to be much larger during nighttime and much smaller during daytime (not shown) at most surface observational sites including CASTNET and SEARCH. The NMBs for WDR10 are within 6% at both CASTNET and SEARCH sites. The west-east component of WSP10 (U10) is overestimated domain-wide with NMBs above 300%. The south-north component of WSP10 (V10) is comparable with CASTNET observations (with an NMB of 13.8%–14.6%) but is significantly overestimated at the SEARCH sites (with an NMB of 133.1%–157.4%). As shown in *Otte* [2008a, 2008b], the use of 4-D data assimilation can reduce the biases in wind predictions.

[18] The impact of different gas-phase mechanisms on meteorological predictions under some conditions at some locations can be sizeable. Figure 3 show temporal variations of SWD, T2, and RH2 at the SEARCH sites to examine differences in simulated aerosol direct, semi-direct, and indirect effects caused by different gas-phase mechanisms. All three gas-phase mechanisms predict very similar SWD under clear-sky conditions at the SEARCH sites, indicating their minor role in the predictions of aerosol direct effect. However, discrepancies of SWD under cloudy-sky conditions among the three simulations could become as large as 500 W m^{-2}, demonstrating an important role of aerosol indirect effect. The impact of cloud radiative forcing (which is affected by aerosol indirect effects) on SWD and the differences among simulated SWD under cloudy conditions could become even larger if CWP and COT are not significantly underpredicted. As an example, the discrepancies of SWD caused by different gas-phase mechanisms are above 100 W m^{-2} on July 28 and 30 (Figure 3), the differences in T2 and RH2 during this time period could become as large as 3°C and 10%, respectively, at all SEARCH sites, reflecting their responses to changes in SWD. Differences in T2, RH2, and SWD among simulations are generally not as large as those between simulated and their receptive observed values, due to the fact that the simulated surface layer meteorological parameters are very similar with different gas-phase mechanisms, but they are quite different from observations.

3.2. Surface Concentrations

[19] Table 5 summarizes performance statistics of chemical predictions. Figure 4 shows simulated and observed spatial distributions of monthly mean maximum 1 h and 8 h O_3 mixing ratios and their NMBs. Surface O_3 mixing ratios are underpredicted over the western United States, especially along the Pacific coastal area, but overpredicted over the eastern United States, especially over Georgia, Kentucky, Tennessee, Alabama, and Mississippi. All simulations give low NMBs for maximum 1 h and 8 h O_3 mixing ratios (2.8%–12.4% and 7%–18.2%, respectively) at the CASTNET and AQS sites but higher NMBs (23.6%–36.8% and 33.3%–46.9%, respectively) at the SEARCH sites (Table 5), due likely to several reasons. For example, the emissions of O_3 precursors (e.g., NO_x) in the southeastern United States may have been overestimated [*Zhang et al.*, 2006b, 2010b; *Liu and Zhang*, 2011]. Shortwave radiation and temperature are overestimated on some days (see SEARCH sites JST, YRK, and PNS in Figure 3), which lead to a stronger photochemistry than what it should be. The vertical mixing at the SEARCH sites may be underestimated. In addition, the use of a coarse horizontal grid resolution of 36 km cannot accurately capture pointwise measurements at urban sites. The discrepancies of maximum 1 h and 8 h O_3 mixing ratios between CBM-Z and CB05 are within ±2 ppb over most of the domain, with CBM-Z predictions slightly higher over the western and eastern United States, and CB05 predictions slightly higher over the central United States. As shown in Figure 4, SAPRC-99 gives higher maximum 1 h and 8 h O_3 over the entire domain than the other two gas-phase mechanisms, with higher values by at least 2 ppb over most of the domain and by 6–11 ppb over the southeastern United States, where large biogenic emissions occur. This is consistent with the findings in *Luecken et al*. [2008]. The inclusion of methacrolein and aromatic aldehydes in SAPRC-99 leads to higher O_3 formation than CB05.

[20] Figure 5 shows simulated mixing ratios of ALD2 (which is a precursor of PAN), HNO_3, PAN and higher PAN analogues (PANs), and the sum of the mixing ratios of HNO_3 and PANs. CBM-Z gives the highest HNO_3 but the lowest ALD2 and PANs; CB05 gives the highest ALD2, PANs, and the sum of HNO_3 and PANs; and SAPRC-99

Figure 2. Spatial distributions of meteorological variables overlaid with available observations. SWD, surface incoming shortwave radiation (overlaid against observations from CASTNET and SEARCH); T2, 2 m temperature (overlaid against observations from CASTNET, STN, and SEARCH); RH2, 2 m relative humidity (overlaid against observations from CASTNET and SEARCH); and WSP10, 10 m wind speed (overlaid against observations from CASTNET and SEARCH) from WRF/Chem-MADRID simulations with CB05. The observational data are indicated by circles.

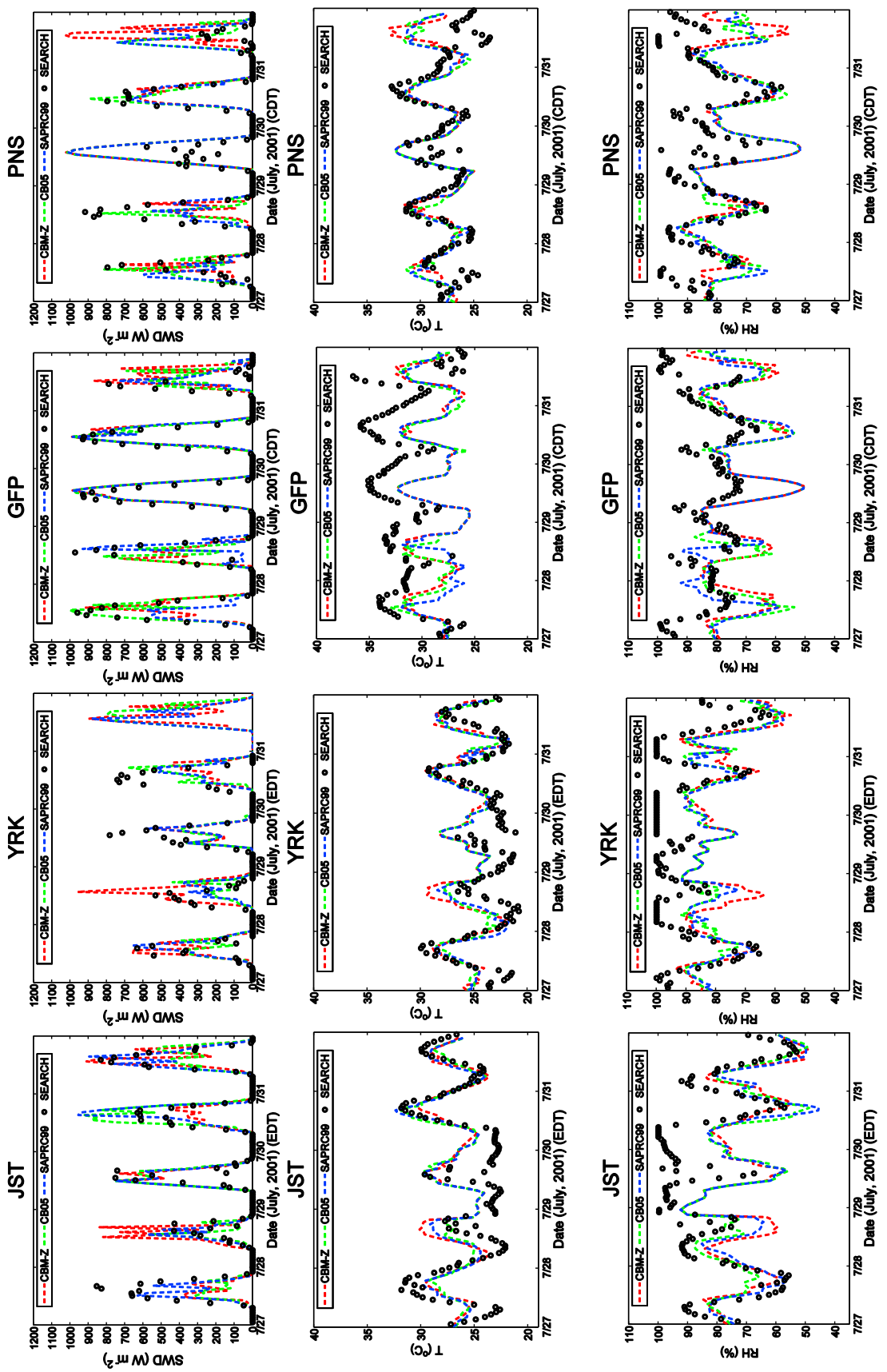

Figure 3. Temporal variation of observed and simulated SWD (row 1), T2 (row 2), and RH2 (row 3) from the simulations with CBM-Z, CB05, and SAPRC-99 during 27–31 July 2001 at 4 SEARCH sites including Jefferson St. (JST), Atlanta, Ga.; Yorkville (YRK), Ga.; Gulfport (GFP), Miss.; and Pensacola (PNS), Florida.

Table 5. Performance Statistics for Chemical Predictions[a]

Variable	Data Source	Data Point	Mean Obs.	Mean Sim.			NMB (%)			NME (%)		
				CBM-Z	CB05	SAPRC-99	CBM-Z	CB05	SAPRC-99	CBM-Z	CB05	SAPRC-99
Maximum 1 h O_3 (ppb)	CASTNET	2316	56.7	59.2	58.3	63.0	4.4	2.8	11.1	23.4	23.4	26.9
	AQS	33182	58.6	62.0	61.1	65.8	5.9	4.3	12.4	25	25	28.3
	SEARCH	245	59.3	73.3	73.4	81.1	23.6	23.9	36.8	30.9	30.3	39.9
Maximum 8 h O_3 (ppb)	CASTNET	2291	50.6	54.9	54.1	58.4	8.7	7.0	15.5	24.4	24.5	28.8
	AQS	33162	51.1	56.9	56.1	60.4	11.4	9.8	18.2	26.4	26.4	30.8
	SEARCH	241	50.9	67.9	67.9	74.8	33.3	33.3	46.9	37.3	36.9	48.2
TOR (DU)	TOMS/SBUV	12000	44.8	42.3	41.8	42.5	−5.6	−6.7	−5.1	10.1	10.8	9.8
CO (ppb)	SEARCH	4858	217.7	203.4	217.8	215.3	−6.6	0.1	−1.1	41.3	43.6	42.8
Col. CO (molec. cm^{-2})[a]	MOPITT	13920	1.3×10^{18}	1.49×10^{18}	1.6×10^{18}	1.6×10^{18}	18.9	25.7	23.7	29.8	34.2	32.6
SO_2 (ppb)	SEARCH	4820	2.1	3.3	3.4	3.3	58.4	64.4	62.9	134.4	139.3	138.3
HNO_3 (ppb)	SEARCH	4758	0.7	1.8	1.3	1.1	165.4	87.6	66.7	197.9	141	123.6
NO_2 (ppb)	SEARCH	725	9.7	8.9	8.5	8.7	−9.0	−12.7	−11.0	76.3	79.1	74.2
Col. NO_2 (molec. cm^{-2})	GOME	13651	1.5×10^{15}	1.73×10^{15}	1.6×10^{15}	1.8×10^{15}	12.0	5.1	17.0	43.1	42.6	44.9
NO (ppb)	SEARCH	4952	2.8	0.3	0.2	0.3	−88.6	−91.2	−90.7	92.3	93.3	93.3
24 h avg. $PM_{2.5}$ ($\mu g\ m^{-3}$)	IMPROVE	1115	7.4	7.6	7.8	7.8	2.4	5.5	6.0	49.1	49.2	50.7
	STN	788	13.2	13.6	12.9	13.4	2.5	−2.2	1.3	47.2	45.3	46.7
	SEARCH	217	16.8	18.9	18.1	18.1	12.6	7.9	7.7	45.8	44	44.3
SO_4^{2-} ($\mu g\ m^{-3}$)	CASTNET	287	4.6	5.2	4.2	4.7	12.5	−8.3	1.0	33.9	31.6	31.3
	IMPROVE	1118	2.5	2.8	2.3	2.5	12.5	−5.9	3.3	58.9	52.7	55.1
	STN	971	5.1	4.9	4.1	4.5	−3.1	−20.2	−11.9	55.1	52.1	52.5
	SEARCH	229	5.7	9.7	8.2	8.9	68.2	43.6	55.4	80.3	67.7	73.5
NO_3^- ($\mu g\ m^{-3}$)	CASTNET	287	0.4	1.2	0.8	0.7	234.9	125.6	87.9	263	167.6	137.5
	IMPROVE	1117	0.3	1.0	0.7	0.6	245.0	159.9	63.9	294.9	218.2	191.6
	STN	727	1.6	2.3	1.7	1.4	39.6	2.8	−16.2	151.9	127.1	113.2
	SEARCH	229	0.3	1.1	0.7	0.5	272.5	127.4	75.5	315.2	204.4	159.7
NH_4^+ ($\mu g\ m^{-3}$)	CASTNET	287	1.4	1.7	1.2	1.2	25.2	−13.0	−8.5	44.1	35.6	35.2
	IMPROVE	30	1.4	2.8	1.9	2.0	103.3	38.4	45.5	114.7	73.1	75.6
	STN	971	2.0	1.7	1.2	1.2	−16.1	−40.8	−39.0	80.4	76	74.8
	SEARCH	224	1.7	3.0	2.2	2.3	83.0	31.2	39.1	94.1	63.9	67.1
BC ($\mu g\ m^{-3}$)	IMPROVE	1126	0.2	0.3	0.3	0.3	31.2	31.7	31.6	64	64.3	64.2
	SEARCH	234	0.8	0.5	0.5	0.5	−40.0	−39.8	−40.2	52.2	52.4	52.2
OM ($\mu g\ m^{-3}$)	IMPROVE	1129	1.7	1.0	2.1	1.9	−42.6	21.3	13.7	56.8	64.9	68.5
	SEARCH	234	4.9	1.3	3.1	2.4	−72.6	−36.1	−50.5	72.9	46.6	55.1
TC ($\mu g\ m^{-3}$)	STN	978	4.4	1.9	2.5	2.7	−57.0	−42.7	−38.8	66.9	60.6	65.8

[a]The statistics of column CO is calculated based on the MOPITT data in August, since no data are available for June and July 2001.

gives the lowest HNO_3. This indicates a more important role of organic chemistry in dictating the nitrogen budget in SAPRC-99 and CB05 than in CBM-Z. The differences in HNO_3 predictions are largely due to a different reaction rate for conversions of NO_2 and N_2O_5 to HNO_3 used in these mechanisms, which are the major pathways for HNO_3 formation in the gas phase during the daytime and nighttime, respectively. For example, at a temperature of 300 K, the reaction rate constants for $NO_2 + OH + M \rightarrow HNO_3$ are the highest in CB05 (~2.9 times greater than that in CBM-Z) and the lowest in SAPRC-99 (~3.9 times lower than that in CBM-Z). The reaction rate constant for $N_2O_5 + H_2O \rightarrow HNO_3$ used in CBM-Z is about 7.7 times greater than that used in SAPRC-99 and that used in CB05 is within 4% of the value used in SAPRC-99. However, CB05 uses an additional reaction for homogeneous hydrolysis of N_2O_5 (i.e., a termolecular reaction involving N_2O_5 and H_2O). Thus, the effective homogeneous hydrolysis rate of N_2O_5 in CB05 at an elevated level of water vapor may be greater than that in SAPRC-99. The high reaction rate constant for $NO_2 + OH + M \rightarrow HNO_3$ and the highest reaction rate constant for $N_2O_5 + H_2O \rightarrow HNO_3$ used in CBM-Z, coupled with the highest OH mixing ratio (see Figure 9), lead to the highest HNO_3 mixing ratios among the three simulations.

[21] All three gas-phase mechanisms give very similar spatial distributions of surface NO_2 (figures not shown), with higher (>0.2 ppb) mixing ratios from SAPRC-99 than from the other two mechanisms over most of the eastern United States. Comparing SAPRC-99 to CB05 (see Figure 6), a stronger oxidation by higher OH radicals simulated by SAPRC-99 leads to lower simulated mixing ratios of isoprene and HCHO than by CB05. The largest discrepancies in their surface NO_2 predictions occur in the northeastern and midwestern U.S., whereas the largest discrepancies in their surface O_3 predictions occur in the southeastern U.S. This is partly because of higher BVOCs emissions in the southeastern U.S. than in the northeastern U.S. that are oxidized by higher OH radicals from SAPRC-99 than from CB05, leading to higher O_3 and larger differences between their O_3 predictions in the southeastern United States. Another reason is due to the fact that O_3 chemistry in the southeastern United States is more NO_x-limited than the northeastern United States due to higher BVOCs emissions. This can be illustrated by the photochemical indicators including H_2O_2/HNO_3, NO_y, O_3/NO_x, O_3/NO_y, O_3/NO_z (where $NO_z = NO_y - NO_x$), formaldehyde (HCHO)/NO_y, and HCHO/NO_2 in Figure 7. O_3 chemistry is considered

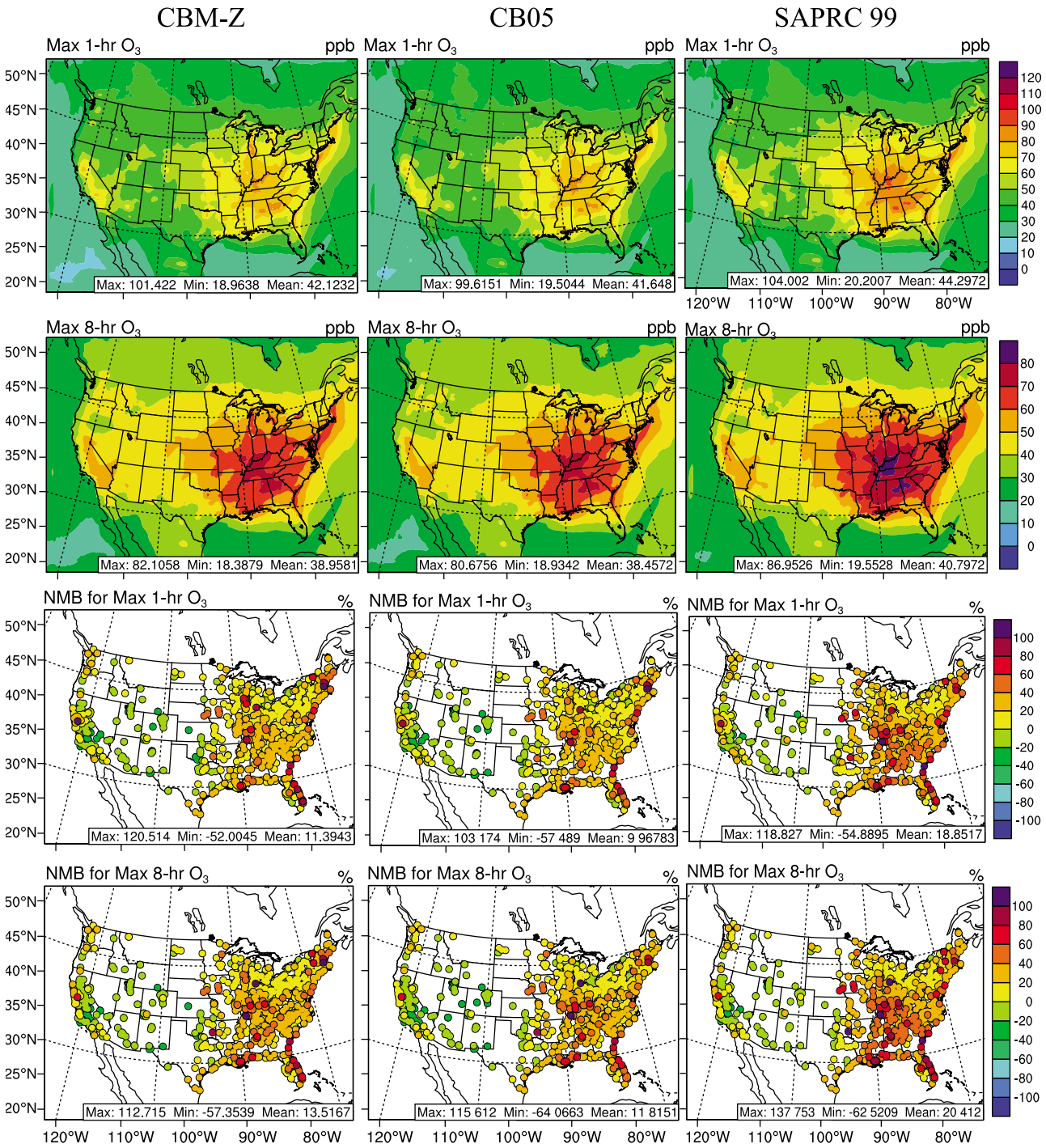

Figure 4. Spatial distributions of maximum 1 h (row 1) and 8 h O_3 mixing ratios (row 2) from WRF/Chem-MADRID simulations with CBM-Z, CB05, and SAPRC-99 gas-phase mechanisms and their normalized mean biases (NMBs) (rows 3 and 4, respectively) calculated using observations from CASTNET, AQS, and SEARCH.

to be NO_x-limited in regions with the values of $H_2O_2/HNO_3 \geq 0.2$, $NO_y \leq 20$, $O_3/NO_x \geq 15$, $O_3/NO_y \geq 7$, $O_3/NO_z \geq 7$, $HCHO/NO_y \geq 0.28$, and $HCHO/NO_2 \geq 1$ [*Milford et al.*, 1994; *Sillman*, 1995; *Sillman et al.*, 1997; *Lu and Chang*, 1998; *Tonnesen and Dennis*, 2000a, 2000b; *Liang et al.*, 2006]. The higher the value of the indicator is for values above their threshold value, the more NO_x limited the region is. One exception is for NO_y, with a lower value indicating a more NO_x limited for values lower than the threshold value. According to these threshold values, O_3 chemistry is NO_x limited in most of domain, although it is VOC limited in big cities such as Los Angeles, Chicago, New York, Houston, and New Orleans. The values of H_2O_2/HNO_3 and O_3/NO_z do not show obviously the VOC limited

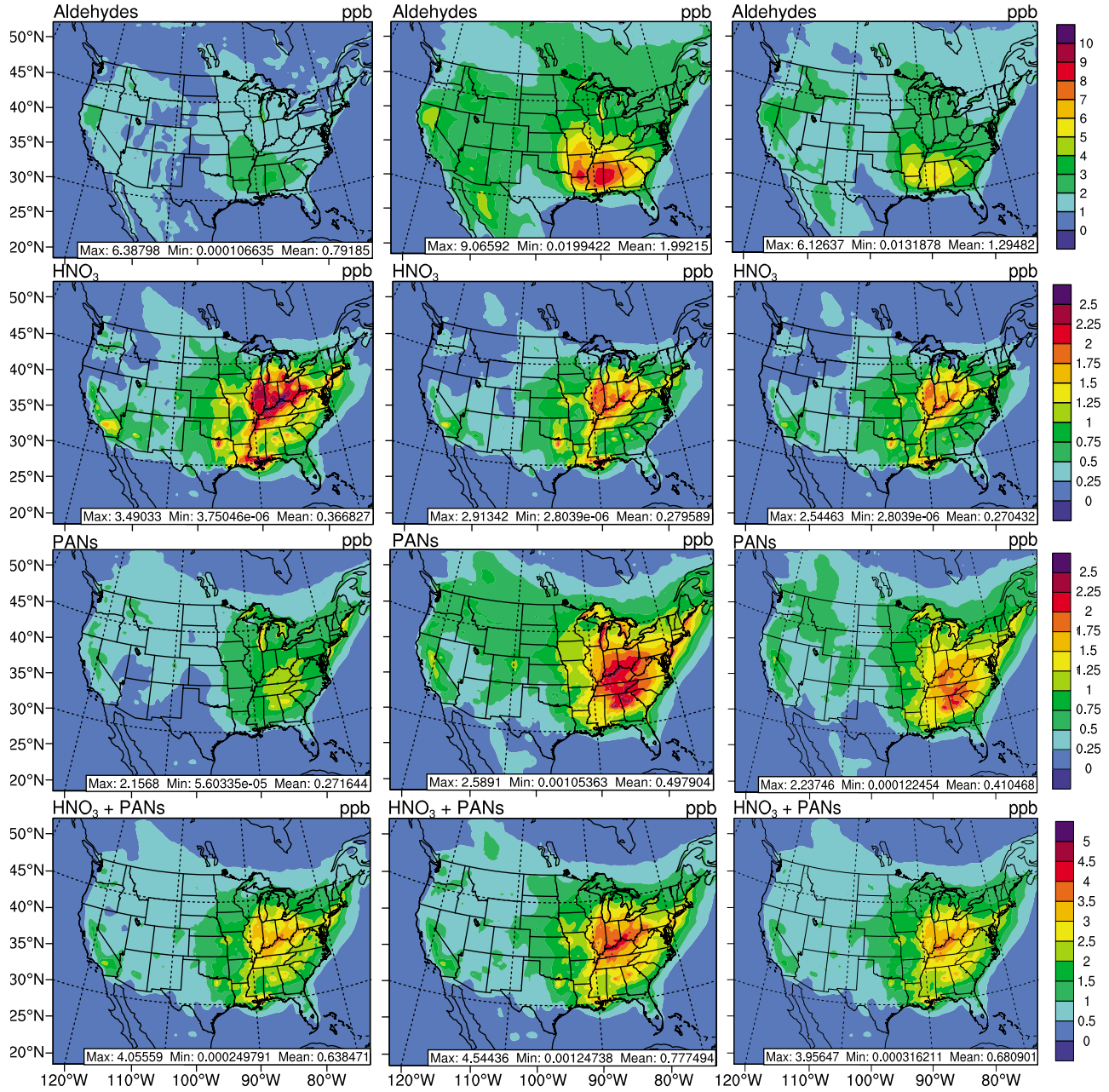

Figure 5. Spatial distributions of ALD2, HNO_3, PANs, and their summation (HNO_3 + PANs) from WRF/Chem-MADRID simulations with (left) CBM-Z, (middle) CB05, and (right) SAPRC-99 gas-phase mechanisms.

O_3 chemistry in those big cities due to several reasons. First, different threshold values under different conditions were proposed to use to indicate VOC or NO_x limited chemistry. For example, a different threshold value of H_2O_2/HNO_3 was proposed to be 0.4 by *Sillman* [1995], 0.8–1.2 by *Lu and Chang* [1998], and 2.4 by *Zhang et al.* [2010b]. Using threshold values of 0.8–1.2 or 2.4, the values of H_2O_2/HNO_3 indicate VOC limited O_3 chemistry in big cities, consistent with results using other indicators. Similarly, O_3/NO_z with a threshold value of 20 as suggested by *Zhang et al.* [2009] also indicates VOC limited O_3 chemistry in some big cities. Second, the use of a low model horizontal resolution of 36 km dilutes urban emissions and artificially changes the O_3 chemistry from a VOC limited nature to a NO_x limited regime. Simulated values of indicators in the southeastern United States are larger (but smaller for NO_y) than those in the northeastern United States, indicating that O_3 chemistry is more NO_x limited in the southeastern U.S. than in the northeastern U.S.

[22] Figure 8 shows spatial distributions of 24 h average mass concentrations of $PM_{2.5}$ and its components as well as 24 h average number concentrations of $PM_{2.5}$ from WRF/Chem-MADRID simulations with three gas-phase mechanisms. Modeling results with all three gas-phase mechanisms reproduce observed $PM_{2.5}$ concentrations well, with NMBs of −2.2% to 12.7% against available surface networks

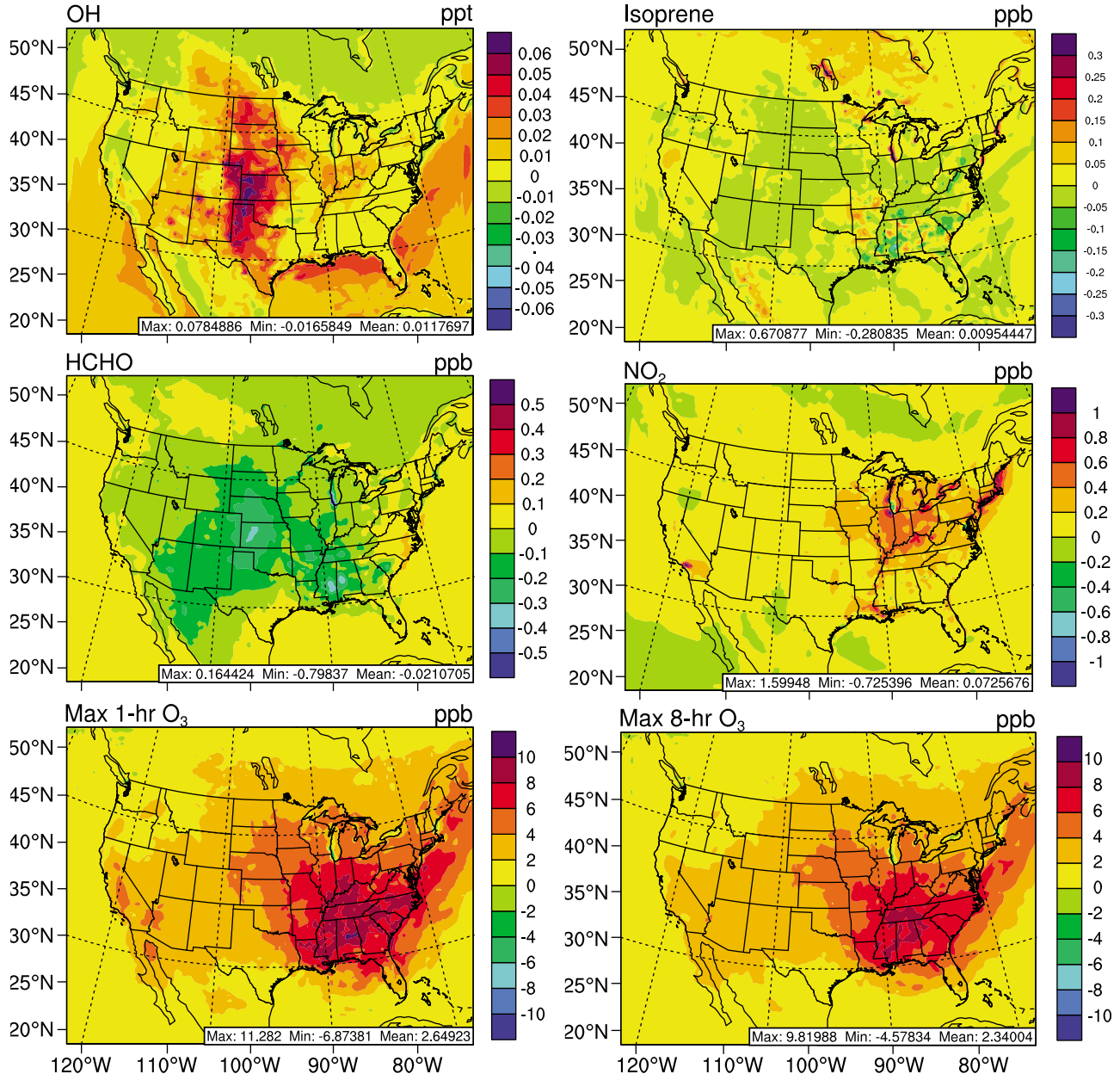

Figure 6. Spatial distributions of differences in mixing ratios of OH, ISOP, HCHO, NO_2, maximum 1 h, and maximum 8 h average O_3, between WRF/Chem-MADRID simulations with SAPRC-99 and CB05 gas-phase mechanisms.

(Table 5). CB05 and SAPRC-99 are more similar in spatial patterns of $PM_{2.5}$ than either of them is with CBM-Z. Compared with statistics shown in *Zhang et al.* [2010b], predictions of $PM_{2.5}$ and its components are noticeably improved because of the use of a positive definite advection scheme. For example, NMBs for $PM_{2.5}$ predictions are 2.4%, 2.5%, 12.6% at the IMPROVE, STN, and SEARCH sites from the simulation with CBM-Z in Table 5, as compared with 8.5%, 21.5%, 33.1%, respectively, from *Zhang et al.* [2010b]. Similar improvements are found for SO_4^{2-}, NO_3^-, and NH_4^+. This is mainly because the simulations in this work are based on WRF/Chem version 3.0, which uses a positive advection scheme and an improved YSU PBL scheme that were not available in WRF/Chem version 2.2 used in *Zhang et al.* [2010b]. The use of these schemes greatly reduces the overpredictions in $PM_{2.5}$ mass concentrations with a more accurate representation of mixing processes in the PBL.

[23] SO_4^{2-} is produced through the gas-phase oxidation of SO_2 by OH, and aqueous-phase oxidation by dissolved oxidants such as H_2O_2. As shown in Figure 9, CBM-Z gives the highest OH, CB05 gives the lowest OH but the highest H_2O_2, and SAPRC-99 gives the lowest H_2O_2. The aqueous-phase SO_2 oxidation is likely being underestimated due to a significant underestimation of CWP (see Figure 1 and Table 4), which is supported by not only the overestimation of SO_2 concentrations (with NMBs of 58.4% $\sim$ 64.4% in Table 5), but also the fact that the spatial distribution of SO_2

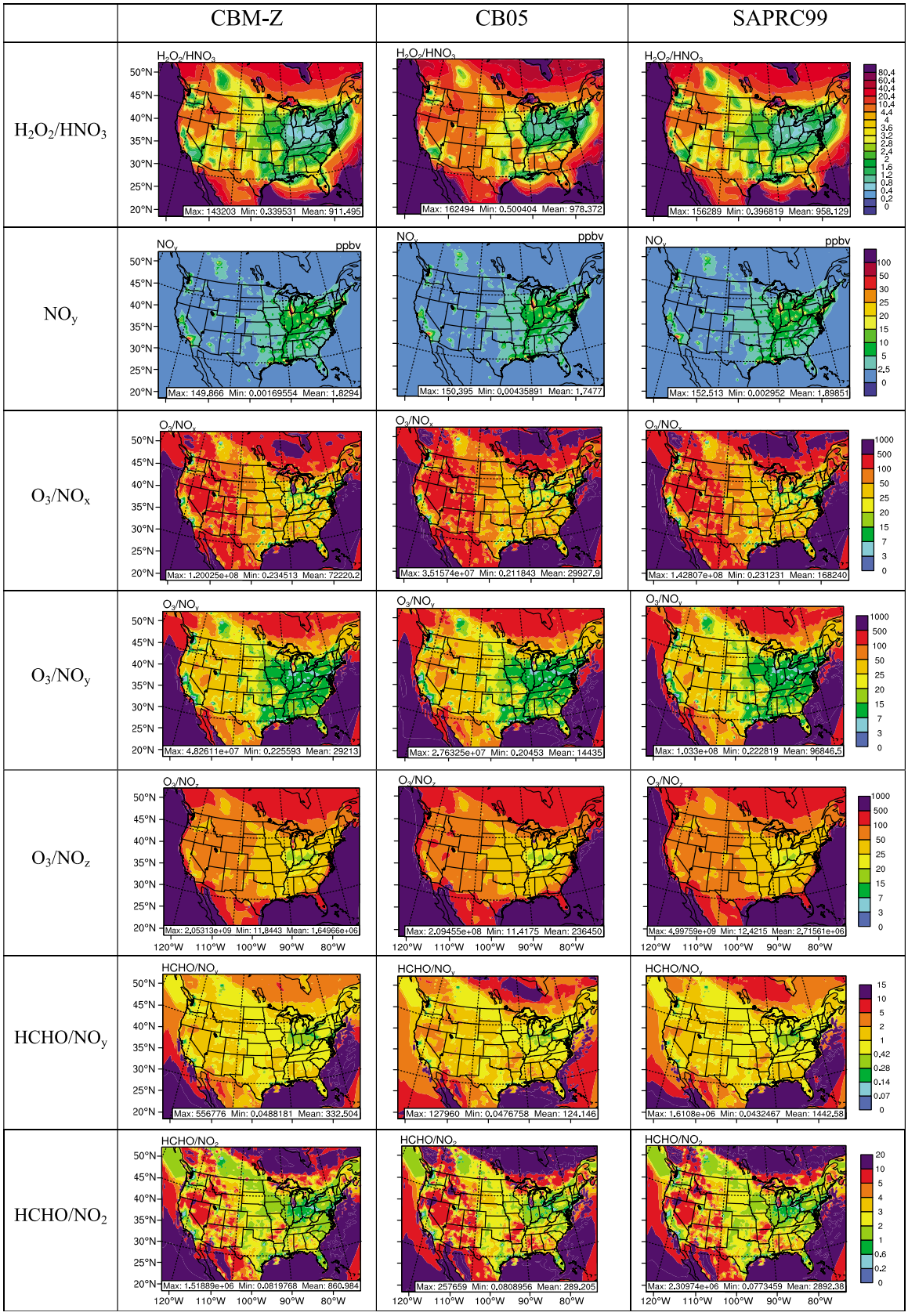

Figure 7. Simulated monthly mean spatial distributions of seven photochemical indicators from WRF/Chem-MADRID simulations with (left) CBM-Z, (middle) CB05, and (right) SAPRC-99 gas-phase mechanisms.

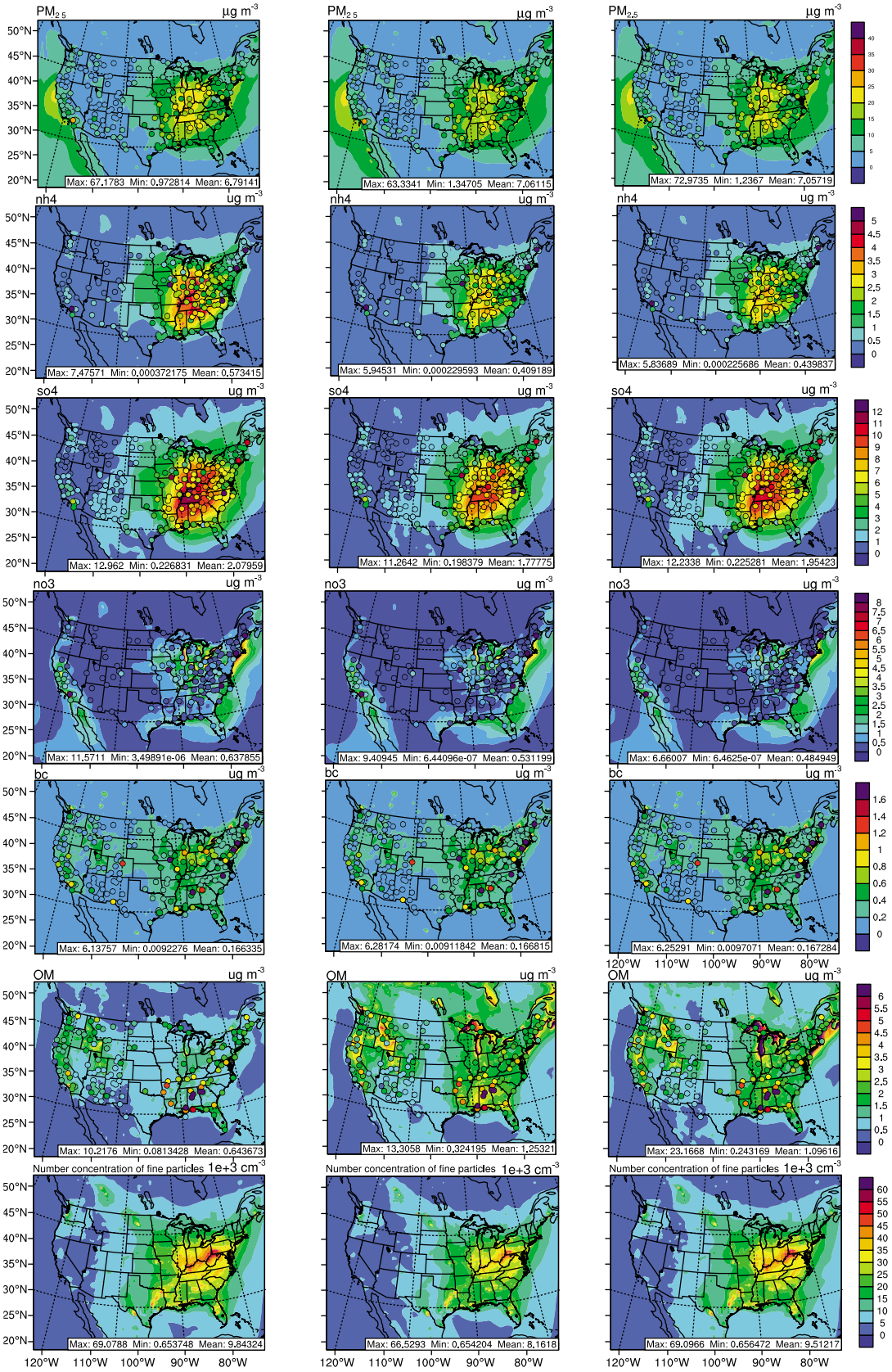

Figure 8. Spatial distributions of 24 h average mass concentrations of $PM_{2.5}$ and its components (overlaid against observations from STN, IMPROVE, and SEARCH) as well as simulated 24 h average number concentrations of $PM_{2.5}$ from WRF/Chem-MADRID simulations with three gas-phase mechanisms: (left) CBM-Z, (middle) CB05, and (right) SAPRC-99.

predictions follows that of OH rather than that of H_2O_2 (not shown). However, since SO_4^{2-} concentrations are dominated by gas-phase oxidation, which may have been overestimated due to overestimated shortwave radiation (with NMBs of 15%–22.7% at the CASTNET and SEARCH sites, see Table 4) and SO_2 emissions (with NMBs of 58.4%–64.4% at the SEARCH sites, see Table 5). The underpredicted aqueous-phase SO_4^{2-} formation does not lead to large underpredictions in SO_4^{2-} concentrations at all network sites, as indicated by their NMBs. Among the three simulations, CBM-Z gives the highest concentrations of SO_4^{2-}, NO_3^-, and NH_4^+, due primarily to the highest mixing ratios of OH. Although CB05 gives much higher H_2O_2 than the other two gas-phase mechanisms, it still gives the highest SO_2 and the lowest SO_4^{2-} due to the simulated dominance of gas-phase oxidation over aqueous-phase oxidation across most of the domain during most time periods. The spatial distribution of NH_4^+ from the three simulations follows that of SO_4^{2-}, because higher SO_4^{2-} concentrations also result in higher NH_4^+ concentrations as a result of the neutralization reactions between them and the fact that high temperatures under summer conditions do not favor the formation of NH_4NO_3. Compared with CB05, SAPRC-99 gives higher concentrations of SO_4^{2-} and NH_4^+ due to higher OH mixing ratios, but lower concentrations of NO_3^- due to lower mixing ratios of HNO_3 resulted from a lower reaction rate for the conversion of N_2O_5 to HNO_3.

[24] NO_3^- concentrations are determined by the concentrations of its precursor HNO_3 and thermodynamic equilibrium involving cations such as NH_4^+ and other anions such as SO_4^{2-} in the particulate phase As shown in Figure 5, simulated HNO_3 mixing ratios are the highest by CBM-Z and the lowest by SAPRC-99, consequently, NO_3^- concentrations are the highest by CBM-Z and the lowest by SAPRC-99 (see Figure 8). All simulations give large overpredictions of NO_3^- concentrations (NMBs of 234.9%–272.5% for CBM-Z, 125.6%–159.9% for CB05, and 63.9%–87.9% for SAPRC-99 in Table 5) at the CASTNET, IMPROVE, and SEARCH sites but much smaller biases (NMBs of 39.6% for CBM-Z, 2.8% for CB05, and −16.2% for SAPRC-99) at the STN sites. The large overprediction in the NO_3^- concentrations can be attributed to three main factors. First, the overprediction in the shortwave radiation may have led to higher HNO_3 photochemical production than what it should be in the gas-phase. Second, the reaction probability (γ) of 0.1 for the heterogeneous reaction of N_2O_5 to produce HNO_3 may be too high. Recent laboratory data reported γ values in the range of 0.002 and 0.02 [*Davis et al.*, 2008, and references therein]. Lower biases at the STN sites indicate that the γ value of 0.1 may be more appropriate at those sites than other network sites. Third, the rate constant for the homogeneous hydrolysis of N_2O_5 used in all mechanisms may be too high. For example, the International Union of Pure and Applied Chemistry (IUPAC) recently suggested a much lower value for the rate constant for the bimolecular hydrolysis of N_2O_5 (www.iupac-kinetic.ch.cam.ac.uk). While some studies showed the anti-correlation between the biases in simulated SO_4^{2-} and NO_3^- (e.g., the systematic underestimations of NO_3^- result from overestimations of SO_4^{2-} for 2004 at the STN, IMPROVE, and CASTNET sites over the eastern United States [*Yu et al.*, 2008], such a correlation is not obvious at the network sites for 2001.

[25] All three gas-phase mechanisms give very similar predictions of BC, with an overprediction of ∼32% at the IMPROVE sites and an underprediction of about 40% at the SEARCH sites, indicating uncertainties in primary carbon emissions and in some atmospheric processes such as vertical mixing, advection, and removal, as BC is not chemically reactive. Compared with WRF/Chem using CBM-Z and MOSAIC in *Zhang et al.* [2010b] that gives NMBs of 68.1% and −14.3% at the IMPROVE and SEARCH sites, simulated BC concentrations in this effort with a more accurate representation of the PBL mixing processes are less overpredicted at the IMPROVE sites but more underpredicted at the SEARCH sites. This indicates that emissions of BC in the urban/rural areas of the eastern United States are likely underestimated and those in the IMPROVE rural or remote locations are likely overestimated. NMBs for OM predictions are −42.6% and −72.6% at the IMPROVE and SEARCH sites from the simulation with CBM-Z/MADRID in this work, as compared with −37.1% and −49.4%, respectively, from CBM-Z/MOSAIC in *Zhang et al.* [2010b]. Note that OM predictions from CBM-Z/MADRID in this work and CBM-Z/MOSAIC in *Zhang et al.* [2010b] are primary OM predictions because of exclusion of SOA. More underpredictions in OM with a more accurate representation of PBL mixing processes in this effort imply again the possible underestimate of primary OM emissions in the eastern United States. Compared with the simulation with CBM-Z, the simulations with CB05 and SAPRC-99 give lower biases in OM because of their inclusion of SOA formation, with 21.3% and 13.7% at the IMPROVE sites, respectively, and −36.1% and −50.5% at the SEARCH sites. Simulated SOA concentrations are mostly in the range of 1–6 μg m^{-3} in the Great Lakes region, 1–2 μg m^{-3} in some areas of the southeastern and northwestern U.S., and <0.5–1 μg m^{-3} in other areas (not shown). Large differences between SOA concentrations simulated with CB05 and SAPRC-99 occur in areas with high emissions of biogenic VOCs and high molecular alkanes. For example, SAPRC-99 gives lower SOA in the southeastern U.S. but higher SOA over the Great Lakes area and the northeastern coast of the U.S. Compared with CB05, SAPRC-99 gives higher predictions of all oxidants, including O_3 (see Figure 4), OH (Figure 6), and O and NO_3 (figures not shown), over most of the domain, which should favor SOA formation. However, CB05 actually gives higher SOA concentrations than SAPRC-99 domain-wide, except at urban sites (e.g., STN) where high molecular alkanes make a significant contribution to SOA formation. This can be attributed to two main reasons. First, SAPRC-99 gives lower mixing ratios of the SOA precursors such as ISOP (see Figure 6), terpenes, and sesquiterpenes in the southeastern U.S. but higher values in the Great Lakes area and the northeastern coastal areas. Second, high molecular alkanes in the Great Lakes region and the northeastern coast can produce additional SOA in SAPRC-99 that is not simulated in CB05. Differences in simulated SOA concentrations dominate differences in simulated organic aerosols by WRF/Chem-MADRID with CB05 and SAPRC-99.

[26] No observations are available for $PM_{2.5}$ number concentrations. Simulated $PM_{2.5}$ number concentrations

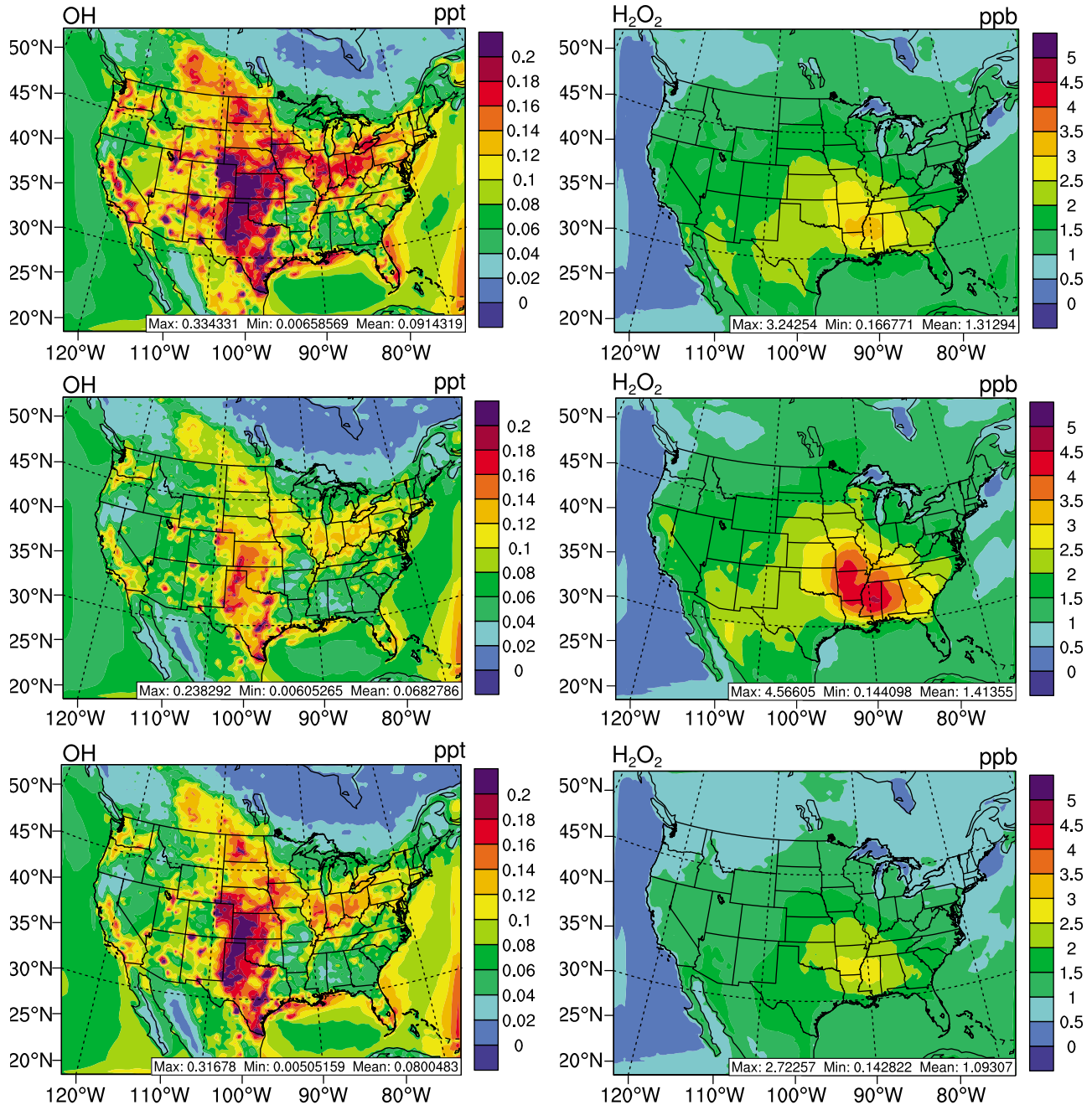

Figure 9. Spatial distributions of OH radical and H_2O_2 from WRF/Chem-MADRID simulations with (top) CBM-Z, (middle) CB05, and (bottom) SAPRC-99 gas-phase mechanisms.

correlate strongly with simulated mass concentrations of SO_4^{2-} and NH_4^+ and thus $PM_{2.5}$ (due to the dominancy of SO_4^{2-} and NH_4^+ among all PM components), with CBM-Z and SAPRC-99 predicting the highest and lowest $PM_{2.5}$ number concentrations, respectively (see Figure 8). The spatial distributions of SO_2 concentrations from the three simulations are very similar (figures not shown), but the concentrations of H_2SO_4 vapor and thus sulfate are quite different due to different levels of OH radical in the gas-phase and oxidants such as H_2O_2 and O_3 in both gas- and aqueous-phase, as shown in Figure 9. Since the rate of new particle formation via homogeneous nucleation is proportional to the availability of H_2SO_4 vapor, a higher H_2SO_4 vapor would lead to a larger nucleation rate. PM number concentrations in the size sections 1–2 (corresponding to the nucleation mode with aerodynamic diameter <0.1 μm in the modal approach) dominate over those in the size sections of 3–6 and 7–8 (corresponding to accumulation (0.1 μm $\leq$ aerodynamic diameter < 2.5 μm) and coarse modes (aerodynamic diameter > 2.5 μm), respectively), contributing to >97% of total PM number concentrations domainwide (figure not shown). A larger nucleation rate will thus result in a larger total $PM_{2.5}$ number concentration, with a larger increase in the PM number concentration in sections 1–2. On the other hand, a higher H_2SO_4 vapor would also lead to a higher condensation rate, thus a larger increase in sulfate

(thus $PM_{2.5}$) mass concentrations mainly in size sections with larger surface areas (i.e., sections 3–6). While increased sulfate mass concentrations due to condensational growth will not directly increase the PM number concentrations in those sections, particles from sections 1–2 locally in this grid cell may grow into sections 3–6 through condensation and coagulation processes and those (regardless of their sizes) in other grid cells may be transported into this grid cell via advection, mixing, and horizontal transport, leading to increases in the PM number concentrations in sections 3–6 (though to a much lesser degree than those in sections 1–2 that dominate the variation trend of $PM_{2.5}$ number concentrations; figures not shown). The simulation with CBM-Z predicts the highest sulfate (and thus $PM_{2.5}$) concentrations, thus the highest $PM_{2.5}$ number concentrations. The strong correlation between $PM_{2.5}$ number and mass concentrations indicates that simulated $PM_{2.5}$ number concentrations are mainly affected by aerosol processes such as new particle formations via homogeneous nucleation and coagulation, although in some cases, the impact of meteorological processes (e.g., such as mixing, advection, and transport) may also be important.

[27] Figures 10–11 show temporal variations of observed and simulated hourly O_3 and $PM_{2.5}$ concentrations at 4 SEARCH sites. All three simulations tend to overpredict O_3 to some extent, with the largest overpredictions occurring at BHM. Among the three simulations, SAPRC-99 gives the highest O_3 mixing ratios at all sites during nearly all time periods. Simulated $PM_{2.5}$ concentrations with all three mechanisms follow the observed variation trends well except for 1–6 July and 24–31 July at all sites, 17 July at JST, YRK, and BHM, and 20 July at CTR, during which overpredictions occur. CBM-Z and CB05 tend to give higher $PM_{2.5}$ concentrations than SAPRC-99 during these time periods.

3.3. Column Variables

[28] Figure 12 shows simulated and observed spatial distributions of column mass concentrations of chemical species and AOD. The corresponding performance statistics are given in Table 4. Unlike surface O_3 concentrations, all three gas-phase mechanisms give very similar TOR predictions (within differences of $\pm 5\%$), indicating that TOR predictions largely depend on O_3 concentrations in upper atmosphere, where boundary conditions play a more important role than atmospheric chemistry. Compared with observations from TOMS/SBUV, TOR is underpredicted over most of the domain, especially over the central United States, and overpredicted along the south lateral boundaries, with domain-wide NMBs of -6.7% to -5.1%. Surface CO predictions agree well with SEARCH observations (see Table 4), while column CO abundance is moderately overpredicted with NMBs of 18.9%–23.7% (note that MOPITT satellite data for August 2001 was used for evaluation, since no MOPITT observations were available for July 2001). CO is affected by emissions, secondary formation through oxidation of VOCs by various radicals (e.g., OH and NO_3) and oxidants (e.g., O_3), among which oxidations by OH (e.g., HCHO + OH) dominate, and the destruction via CO + OH reaction. All three simulations use the same emissions, the differences in simulated CO via chemical reactions are therefore mainly responsible for differences in simulated surface and column CO mixing ratios. Highest OH mixing ratios simulated by CBM-Z lead to the lowest CO mixing ratios and the lowest NMB among the three simulations, whereas CB05 gives the highest CO column due to the lowest OH mixing ratios and thus the largest NMB. Despite moderate domainwide NMBs of 19%–26%, the simulated spatial distributions of CO mixing ratios agree poorly with observations from MOPITT. Column NO_2 abundance is underpredicted in the western United States, especially along the Pacific coastal area, and overpredicted in the eastern United States, with the lowest NMB of 5.1% by CB05. The simulations with different gas-phase mechanisms give overall similar AOD in terms of spatial distribution but somewhat differ in their magnitudes in some areas. Similar to $PM_{2.5}$, CB05 and SAPRC-99 are more similar in spatial patterns of AOD than either of them is with CBM-Z, with domain-wide mean differences of <0.5%. Differences of 10%–30% are found in simulated AOD between CB05 and CBM-Z and between SAPRC-99 and CBM-Z in the Great Plains and Pacific Northwest. The magnitude of predicted AOD from three simulations is comparable to MODIS observations with domain-wide NMBs of 2.5%–7.2%, but AOD is overpredicted over the eastern United States, and underpredicted over the western United States, for all three gas-phase mechanisms.

[29] Figure 13 shows the spatial distributions of CCN at a superstation (S) of 0.5% and CDNC. CCN observations are only available over ocean. CCN concentrations are significantly overpredicted by simulation results with all three gas-phase mechanisms with NMBs of 178.7%–263.1%, especially over Atlantic. This is due to too high PM concentrations over most oceanic areas and some coastal areas that may be caused by too strong horizontal transport of continental polluted air that contains high PM mass and number concentrations to these areas and too large production of sea salt over these oceanic areas (both are indicated by large overpredictions of wind speeds) (note that no PM observations over oceanic areas are available for model validation). CDNC is underpredicted by simulation results with all three gas-phase mechanisms (with NMBs of -47.4% to -36.9%), especially over the Midwest and upper Great Plains, as well as the Pacific Ocean. This may be mainly due to large underestimate in cloud amount and inaccuracies in simulated cloud spatial distributions (see CF, COT, and CWP in Figure 1 and Table 4). Figure 14 shows percentage differences in simulated $PM_{2.5}$ number concentrations, CCN, and CDNC between the three simulations. As discussed previously and also shown in Figure 8, simulated $PM_{2.5}$ number concentrations are strongly correlated with simulated sulfate and $PM_{2.5}$ mass concentrations. Simulated $PM_{2.5}$ number concentrations by CB05 are lower by up to 36% and 41% than CBM-Z and SAPRC-99, respectively, due to lower sulfate and $PM_{2.5}$ mass concentrations. Since CCN depends primarily on PM number concentrations and CDNC depends strongly on CCN according to the aerosol activation parameterization of *Abdul-Razzak and Ghan* [2002], the simulation with CB05 gives lower CCN concentrations than those with CBM-Z and SAPRC-99 (e.g., lower by up to 46.5% and 58%, respectively) and the lowest CDNC. The simulation with CBM-Z gives the highest $PM_{2.5}$ mass and number concentrations thus the highest CCN and CDNC concentrations. Higher CDNC would result in a higher cloud

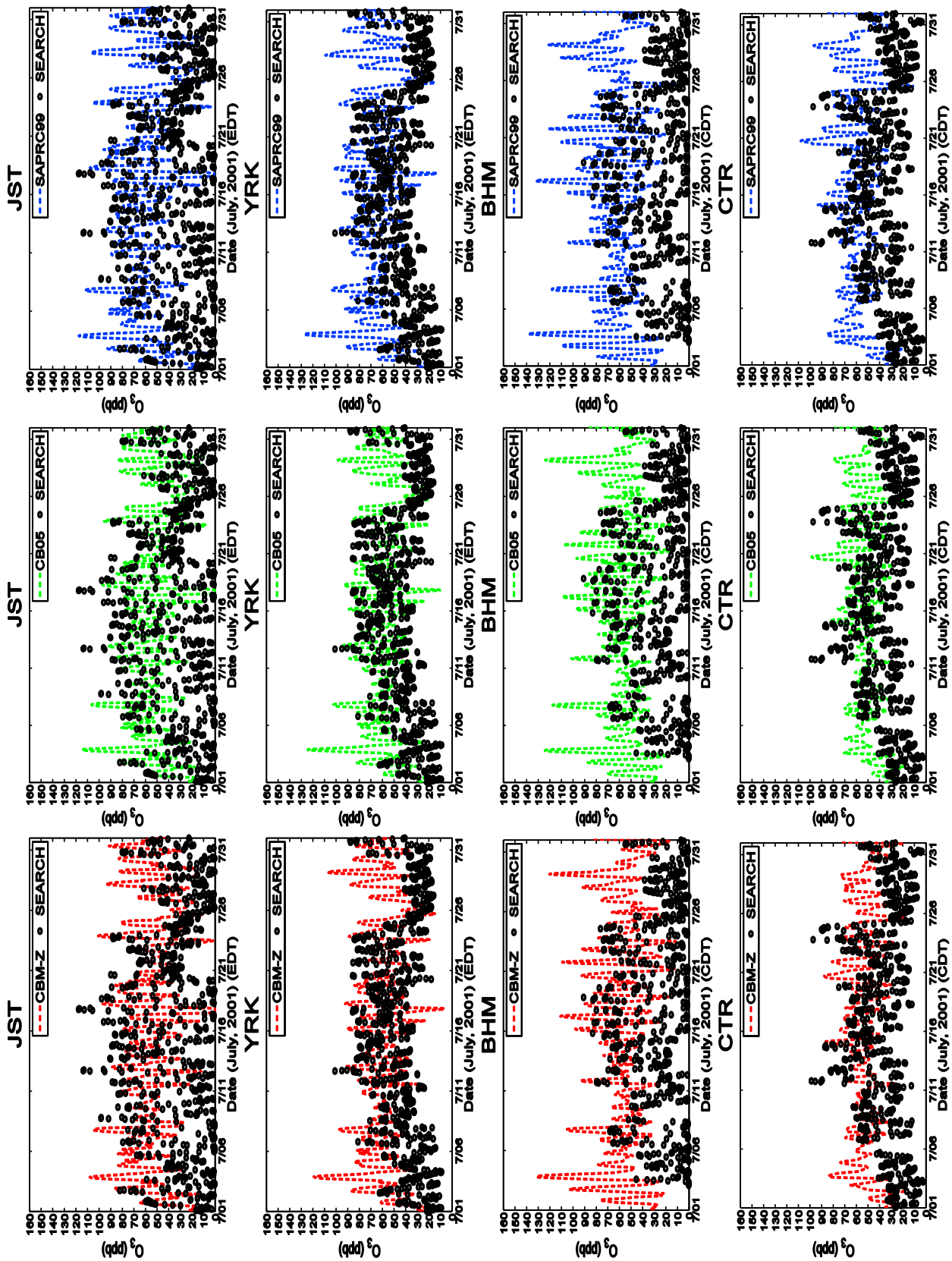

Figure 10. Temporal variation of observed and simulated hourly O_3 mixing ratios from the simulations with CBM-Z, CB05, and SAPRC-99 at 8 SEARCH sites including JST; YRK; North Birmingham (BHM), Ala.; Centreville (CTR), Ala.; GFP; Oak Grove (OAK), Miss.; PNS; and Outlying Landing Field (OLF), Pensacola, Fla.

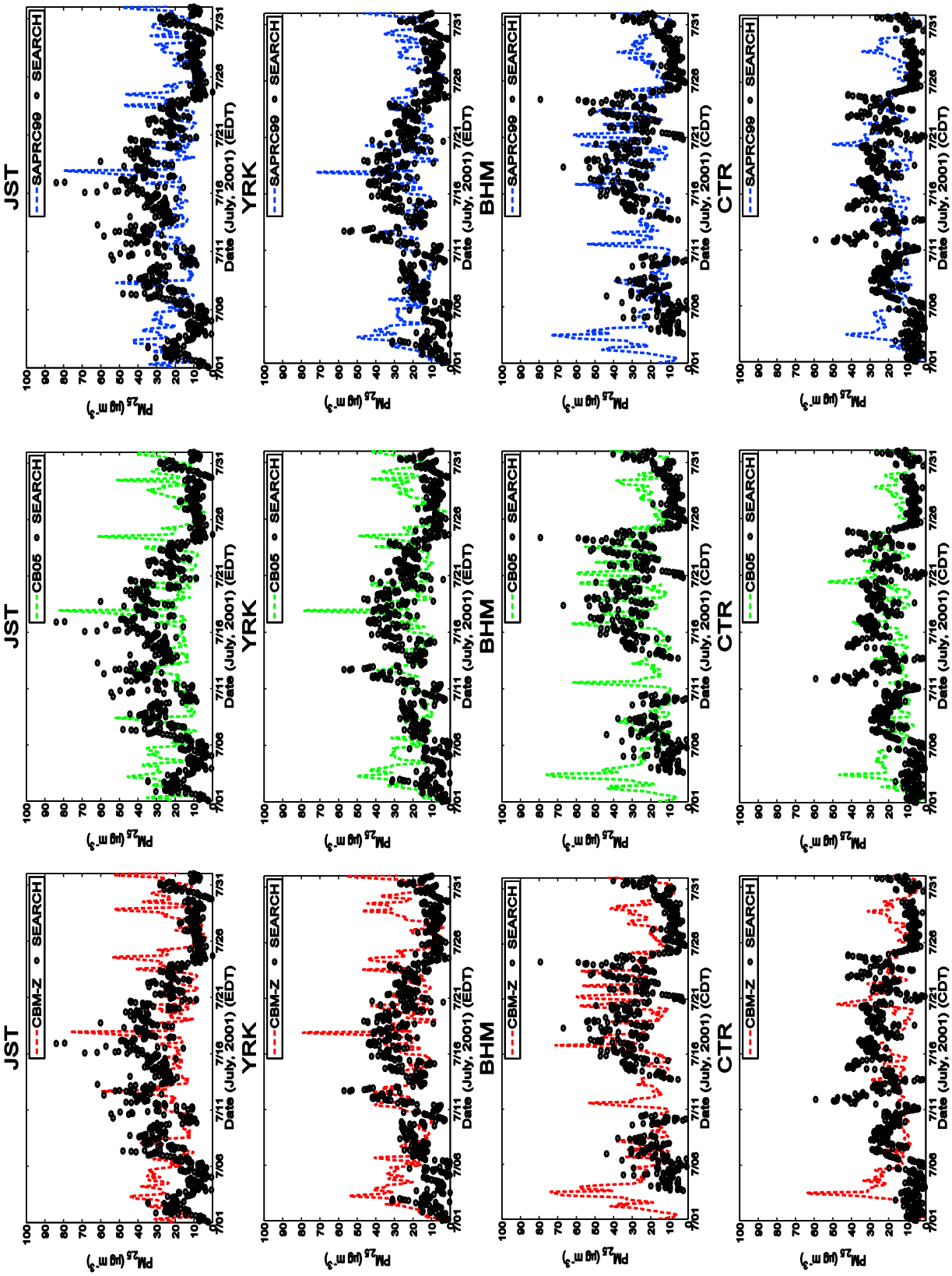

Figure 11. Temporal variation of observed and simulated hourly $PM_{2.5}$ concentrations from the simulations with CBM-Z, CB05, and SAPRC-99 at 8 SEARCH sites including JST, YRK, BHM, CTR, GFP, OAK, PNS, and OLF.

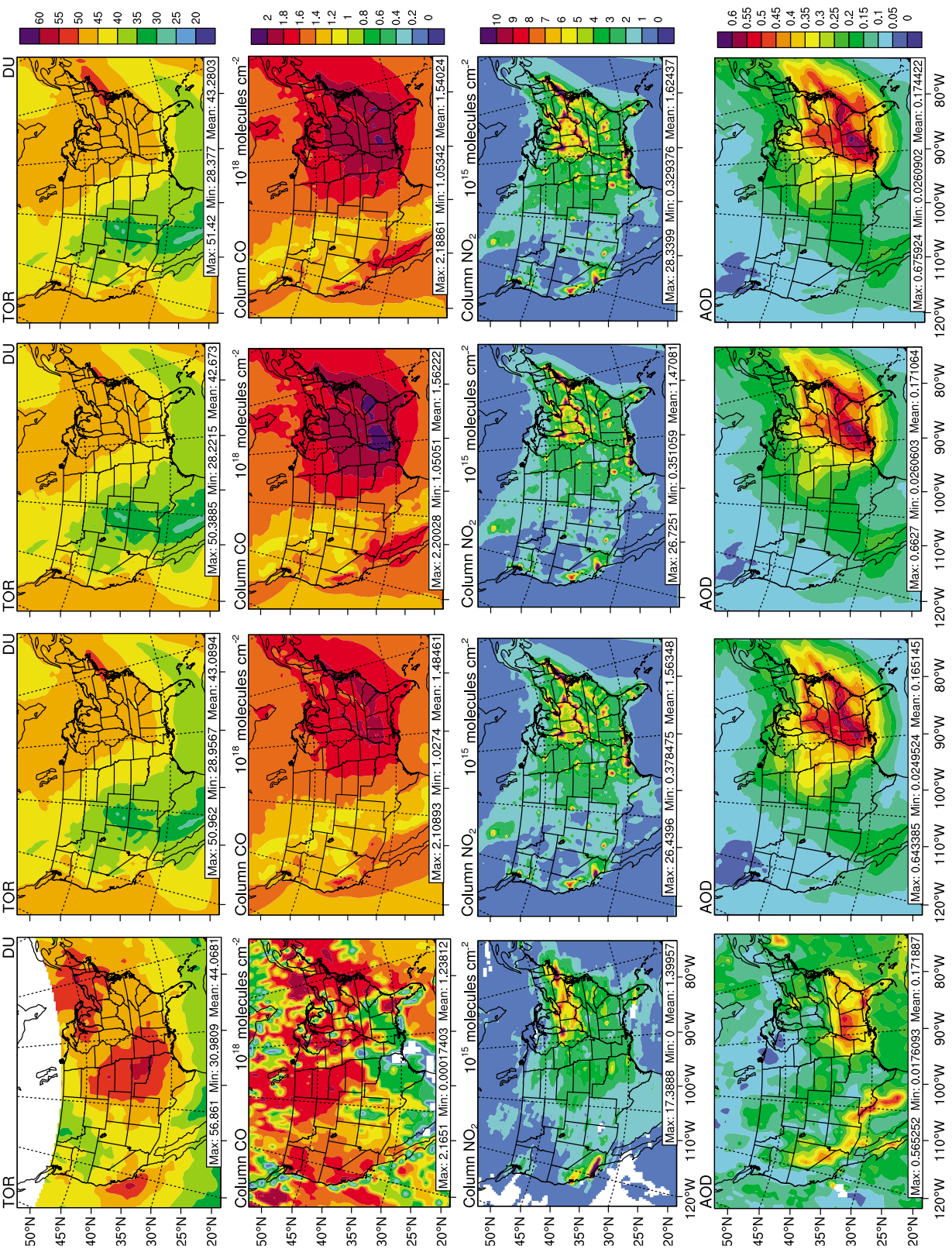

Figure 12. Spatial distributions of column variables. From rows 1 to 4: tropospheric ozone residual (TOR), column CO, column NO_2, and aerosol optical depth (AOD) from satellite data (first column) including TOMS/SBUV, MOPITT, GOME, and MODIS, respectively, and WRF/Chem-MADRID simulations with the gas-phase mechanisms of CBM-Z (second column), CB05 (third column), and SAPRC-99 (fourth column).

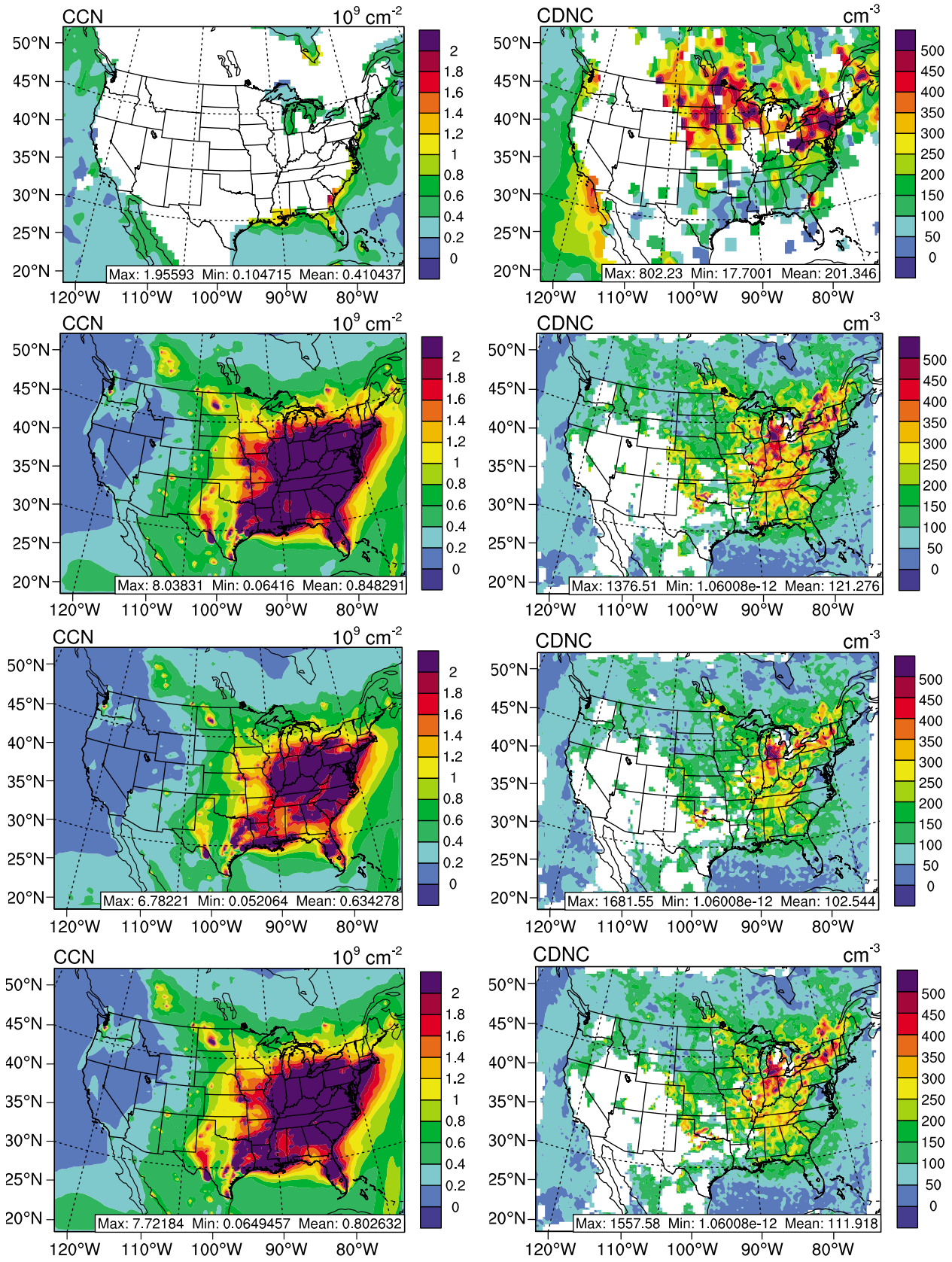

Figure 13. Spatial distributions of cloud condensation nuclei (CCN) concentration and cloud droplet number concentration (CDNC) in warm cloud from satellite data (row 1) including MODIS and *Bennartz* [2007], respectively, and WRF/Chem-MADRID simulations with CBM-Z (row 2), CB05 (row 3), and SAPRC-99 (row 4) gas-phase mechanisms.

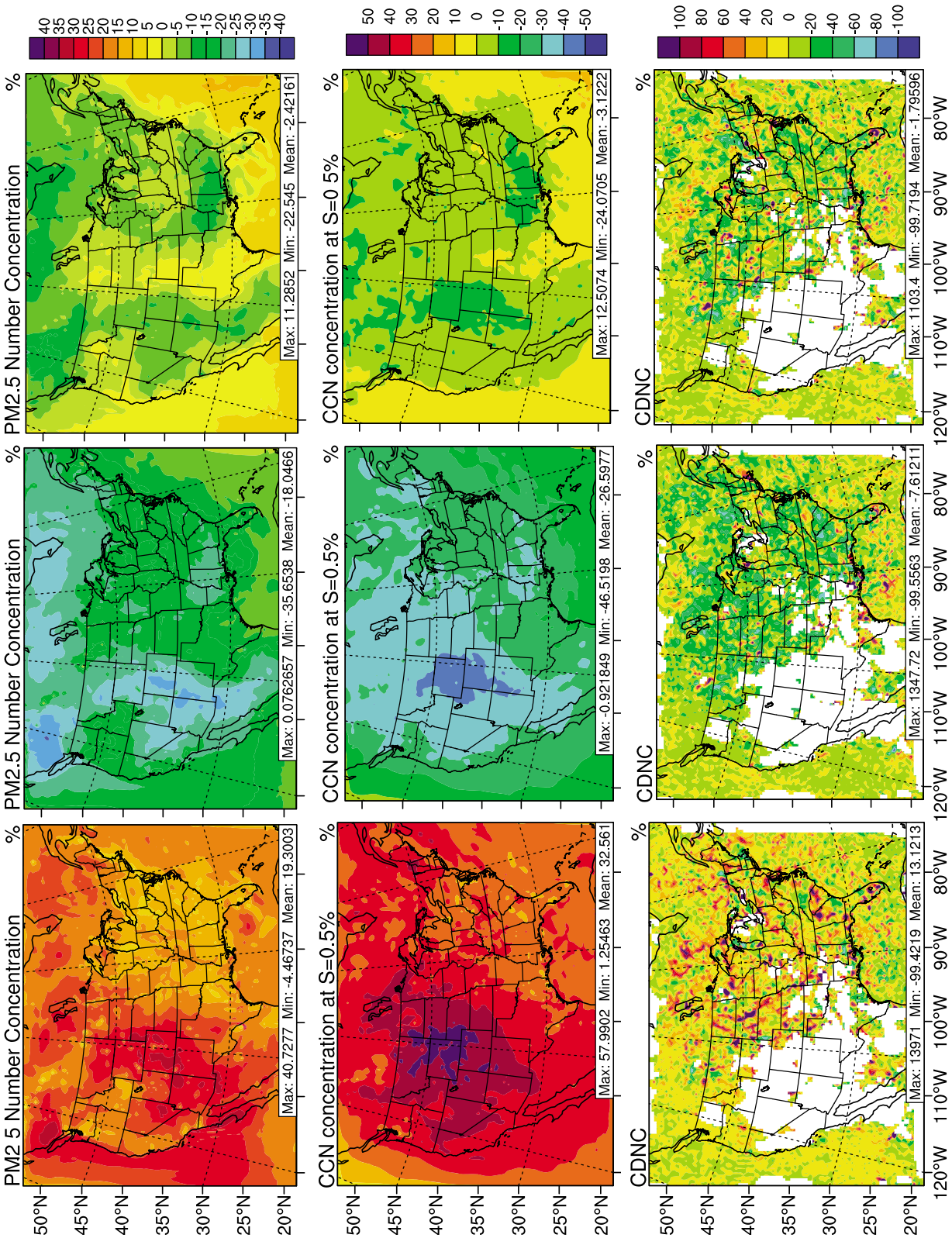

Figure 14. Percentage differences in simulated $PM_{2.5}$ number concentrations, CCN, and CDNC between SAPRC-99 and (left) CB05, (middle) CB05 and CBM-Z, and (right) SAPRC-99 and CBM-Z.

reflectivity, and consequently higher COTs, as shown in Table 4.

4. Conclusions

[30] The WRF/Chem-MADRID simulations with three different gas-phase mechanisms (i.e., CBM-Z, CB05, and SAPRC-99) are conducted over the continental United States for July 2001. Simulation results are evaluated against available surface networks, reanalysis data, and satellite data. All simulations with the three gas-phase mechanisms predict overall similar meteorological predictions domain-wide. The observed surface pressure, temperature at 2 m, relative humidity at 2 m, precipitable water vapor, and cloud fraction are well reproduced with NMBs <15%. SWD is moderately overpredicted and CWP and consequently COT are significantly underpredicted, indicating larger uncertainties in predictions of shortwave and longwave radiative fluxes. Larger biases occur for simulated WSP10 and precipitation (with NMBs of 49%–98% and 53%–55.6%, respectively), due mainly to limitations in the Monin-Obukhov surface layer parameterization, the YSU PBL scheme, and the Grell-Devenyi ensemble cumulus parameterization. Simulations with different gas-phase mechanisms lead to differences in SWD, T2, and RH2 as large as 500 W m^{-2}, 3°C, and 10%, respectively, during cloudy periods, indicating the importance of aerosol semi-direct and indirect effects on SWD and PBL meteorological variables.

[31] Simulations with all three gas-phase mechanisms well reproduce surface concentrations of O_3, CO, NO_2, and $PM_{2.5}$ and column variables including column CO, column NO_2, TOR, and AOD in terms of domain mean statistics, but cannot reproduce the observed spatial distributions of column CO, TOR, and AOD. The simulation with CB05 gives the best overall predictions of surface level concentrations of CO, O_3, $PM_{2.5}$ and its composition, column NO_2, CCN, and CDNC, that with CBM-Z gives the best overall predictions of SO_2, and NO_2, and that with SAPRC-99 gives the best overall predictions of HNO_3. Although the simulations with CBM-Z and CB05 give very similar predictions of O_3 and NO_2 mixing ratios, their mixing ratios of HNO_3, ALD2, PANs, OH, and H_2O_2 differ significantly. Differences in the conversion rates of N_2O_5 to HNO_3 among the three mechanisms are found to be a major source of uncertainties in chemical predictions. The simulation with SAPRC-99 predicts higher levels of O_3 and NO_2 than do those with the other two gas-phase mechanisms. The area with the largest differences in NO_2 occur to the north of the area with the largest differences in O_3, due to high BVOC emissions in the southeastern United States and the fact that this region is more NO_x limited than the northeastern United States. The differences in the reaction rate to convert N_2O_5 to HNO_3 used by the different gas-phase mechanisms play a major role in the discrepancies of HNO_3 and consequently NO_3^-. Due to the fact that CWP is significantly underpredicted by the model, the role of aqueous-phase SO_2 oxidation is not as significant as it should be, but the underpredicted aqueous-phase SO_4^{2-} formation does not lead to large underpredictions in SO_4^{2-} concentrations at all network sites. All simulations overpredict NO_3^- concentrations due to an overestimate in shortwave radiation, the use of an upper limit value for reaction probability of heterogeneous hydrolysis, as well as a higher rate constant for the homogeneous hydrolysis reaction of N_2O_5 with H_2O to form HNO_3. The simulation with CBM-Z significantly underpredicts OM at the IMPROVE, SEARCH, and STN sites due to an underestimate of primary OM emissions and the lack of SOA treatment in its current implementation in WRF/Chem version 3.0. The simulations with CB05 and SAPRC-99 give better agreement of simulated OM concentrations with observations, due to an inclusion of SOA, which dominates their differences in simulated OM concentrations. Compared with CB05, although SAPRC-99 predicts higher concentrations of all oxidants including O_3, OH, O, and NO_3 than CB05 that would favor SOA formation, it does not always give higher OM, implying other important mechanisms may be important in SOA formation such as in-cloud SOA or removal processes. Differences in aerosol mass and number concentrations resulting from the different gas-phase mechanisms lead to large differences in simulated CCN and CDNC due to the feedback mechanisms among H_2SO_4 vapor, $PM_{2.5}$ number, CCN, and CDNC through gas-phase chemistry, new particle formation via homogeneous nucleation, aerosol growth, and aerosol activation by cloud droplets. Differences in CDNC may impact simulated cloud thickness, cloud albedo, and precipitation.

[32] Cloud microphysics and surface layer parameterizations are two major sources of uncertainties in meteorological simulation. Improvements in predictions of CWP and COT would reduce the uncertainties in aqueous-phase chemistry and photolytic reaction rate constants, and give a more representative magnitude of the aerosol indirect effect. Improvements in predictions of precipitation would also reduce the uncertainties in wet scavenging. On the other hand, improvements in surface layer parameterization, especially under stable conditions, would reduce the uncertainties in predictions of 10-m wind speed as well as exchanges of energy and water vapor between land surface and atmosphere, resulting in more representative responses of other meteorological variables (e.g., T2 and RH2) to differences in shortwave radiation.

[33] As shown in this study, the use of different gas-phase mechanisms leads to appreciable differences in simulated mass concentrations of O_3 (up to 5 ppb), $PM_{2.5}$ (up to 0.5 μg m^{-3}), secondary inorganic $PM_{2.5}$ species (up to 1.1 μg m^{-3}), organic PM (up to 1.8 μg m^{-3}), and the number concentration of $PM_{2.5}$ (up to 2×10^4 cm^{-3}). Such differences cause differences in hourly meteorological variables during cloudy periods through various feedback processes simulated in WRF/Chem that will in turn affect meteorological and chemical predictions as well as aerosol direct and indirect effects during the next step simulation and the average model predictions over the simulation period. Given the non-negligible impact of gas-phase mechanisms on chemical and aerosol predictions and their subsequent effects on meteorological variables and the fact that most air quality models for regulatory applications currently do not account for such feedbacks, the online coupled models that accurately simulate feedbacks between meteorological variables and chemical species will have advantages over traditional offline models in representing the real atmosphere in which such feedbacks occur. They may provide more accurate predictions for regulatory applications. In addition, the online

coupled models can be applied to simulate chemistry-climate feedbacks over a longer period of time to obtain climatological trends on a regional or global scale, thus providing scientific information that can be used to develop effective emission control strategies in support of policy-making for co-benefits of air quality control and climate change mitigation. The importance of these impacts indicates a need for an accurate representation of those feedbacks through various atmospheric processes. This study also demonstrates the skill of WRF/Chem-MADRID with CB05 in reproducing major meteorological variables including pressure, temperature, and moisture, and chemical species including O_3 and $PM_{2.5}$. It is being applied for real time air quality forecasting in the southeastern United States [*Chuang et al.*, 2011; *N. Zhang et al.*, 2011]. In addition, WRF/Chem-MADRID with CB05 for global extension (CB05_GE) [*Karamchandani et al.*, 2011], which is based on WRF/Chem-MADRID with CB05, has been incorporated in a global-through-urban version of WRF/Chem (GU-WRF/Chem). GU-WRF/Chem is being applied in global-through-urban simulations of air quality-climate interactions (Y. Zhang et al., manuscript in preparation).

[34] **Acknowledgments.** This work was supported by the NSF Award Atm-0348819, the Memorandum of Understanding between the U. S. EPA and NOAA under agreement DW13921548, and the U.S. EPA Science to Achieve Results (STAR) program (Grant R83337601). The authors thank Alice Gilliland, Steve Howard, and Shaocai Yu of the U.S. EPA for providing observations from surface monitoring networks and Fortran codes for statistical calculation; Andreas Richter of the University of Bremen, Germany, for providing GOME NO_2 data; Hilary E. Snell of AER, Inc., for processing GOME NO_2; Jack Fishman and John K. Creilson of NASA Langley Research Center for providing TOMS/SBUV TOR data; R. Bennartz of the Department of Atmospheric and Oceanic Sciences, University of Wisconsin, Wisconsin, for providing derived CDNC data based on MODIS measurements; and Ying Pan, a former graduate student at NCSU, for her work on WRF/Chem simulations and postprocessing work. This manuscript has been subjected to U.S. EPA review and approved for publication.

References

Abdul-Razzak, H., and S. J. Ghan (2002), A parameterization of aerosol activation. 3. Sectional representation, *J. Geophys. Res.*, *107*(D3), 4026, doi:10.1029/2001JD000483.

Arteta, J., S. Cautenet, M. Taghavi, and N. Audiffren (2006), Impact of two chemistry mechanisms fully coupled with mesoscale model on the atmospheric pollutants distribution, *Atmos. Environ.*, *40*, 7983–8001, doi:10.1016/j.atmosenv.2006.06.050.

Audiffren, N., E. Buisson, S. Cautenet, and N. Chaumerliac (2004), Photolytic impact of a stratocumulus cloud layer upon the chemistry of an offshore advected plume of pollutants during the NARE 1993 intensive experiment: A numerical study, *Atmos. Res.*, *70*, 89–108, doi:10.1016/j.atmosres.2004.01.004.

Bennartz, R. (2007), Global assessment of marine boundary layer cloud droplet number concentration from satellite, *J. Geophys. Res.*, *112*, D02201, doi:10.1029/2006JD007547.

Binkowski, F. S., and S. J. Roselle (2003), Models-3 Community Multiscale Air Quality (CMAQ) model aerosol component: 1. Model description, *J. Geophys. Res.*, *108*(D6), 4183, doi:10.1029/2001JD001409.

Boersma, K. F., H. J. Eskes, and E. J. Brinksma (2004), Error analysis for tropospheric NO_2 retrieval from space, *J. Geophys. Res.*, *109*, D04311, doi:10.1029/2003JD003962.

Brulfert, G., C. Chemel, E. Chaxel, and J. P. Chollet (2005), Modelling photochemistry in alpine valleys, *Atmos. Chem. Phys.*, *5*, 2341–2355, doi:10.5194/acp-5-2341-2005.

Byun, D., and K. L. Schere (2006), Review of the governing equations, computational algorithms, and other components of the Models-3 Community Multiscale Air Quality (CMAQ) modeling system, *Appl. Mech. Rev.*, *59*, 51–77, doi:10.1115/1.2128636.

Carter, W. P. L. (2010), Development of the SAPRC-07 chemical mechanism, *Atmos. Environ.*, *44*, 5324–5335, doi:10.1016/j.atmosenv.2010.01.026.

CASTNET (2005), *Clean Air Status and Trends Network (CASTNET) 2004 Annual Report*, 72 pp., MACTEC Eng. and Consult. for U.S. Environ. Prot. Agency, Washington, D. C. [Available at http://epa.gov/castnet/javaweb/docs/annual_report_2004.pdf.]

Chapman, E. G., W. I. Gustafson Jr., R. C. Easter, J. C. Barnard, S. J. Ghan, M. S. Pekour, and J. D. Fast (2009), Coupling aerosol-cloud-radiative processes in the WRF-Chem model: Investigating the radiative impact of elevated point sources, *Atmos. Chem. Phys.*, *9*, 945–964, doi:10.5194/acp-9-945-2009.

Chen, F., and J. Dudhia (2001), Coupling an advanced land surface–hydrology model with the Penn State-NCAR MM5 modeling system. Part I: Model implementation and sensitivity, *Mon. Weather Rev.*, *129*, 569–585, doi:10.1175/1520-0493(2001)129<0569:CAALSH>2.0.CO;2.

Chen, S.-H., and W.-Y. Sun (2002), A one-dimensional time dependent cloud model, *J. Meteorol. Soc. Jpn.*, *80*, 99–118, doi:10.2151/jmsj.80.99.

Chen, S., X. Ren, J. Mao, Z. Chen, W. H. Brune, B. Lefer, B. Rappenglück, J. Flynn, J. Olson, and J. H. Crawford (2009), A comparison of chemical mechanisms based on TRAMP-2006 field data, *Atmos. Environ.*, *44*, 4116–4125, doi:10.1016/j.atmosenv.2009.05.027.

Chou, M.-D., and M. J. Suarez (1999), *A Solar Radiation Parameterization for Atmospheric Studies*, *Tech. Rep. Ser. on Global Model. and Data Assimilation*, vol. 15, *NASA/TM-1999-104606*, 51 pp., NASA Goddard Space Flight Cent., Greenbelt, Md.

Chou, M. D., M. J. Suarez, C. H. Ho, M. M. H. Yan, and K. T. Lee (1998), Parameterizations for cloud overlapping and shortwave single-scattering properties for use in general circulation and cloud ensemble models, *J. Clim.*, *11*, 202–214, doi:10.1175/1520-0442(1998)011<0202:PFCOAS>2.0.CO;2.

Chuang, M.-T., Y. Zhang, and D.-W. Kang (2011), Application of WRF/Chem-MADRID for real-time air quality forecasting over the Southeastern United States, *Atmos. Environ.*, *45*, 6241–6250, doi:10.1016/j.atmosenv.2011.06.071.

Davis, J. M., P. V. Bhave, and K. M. Foley (2008), Parameterization of N_2O_5 reaction probabilities on the surface of particles containing ammonium, sulfate, and nitrate, *Atmos. Chem. Phys.*, *8*, 5295–5311, doi:10.5194/acp-8-5295-2008.

Deeter, M. N., D. P. Edwards, J. C. Gille, and J. R. Drummond (2009), CO retrievals based on MOPITT near-infrared observations, *J. Geophys. Res.*, *114*, D04303, doi:10.1029/2008JD010872.

Derwent, R. G. (1990), Evaluation of a number of chemical mechanisms for their application in models describing the formation of photochemical ozone in Europe, *Atmos. Environ., Part A*, *24*, 2615–2624.

Derwent, R. G. (1993), Evaluation of the chemical mechanism employed in the EMEP photochemical oxidant model, *Atmos. Environ., Part A*, *27*, 277–279.

Desert Research Institute (DRI) (2002a), Performance audit of meteorological instruments, *DRI SOP #4-104.2*, Desert Res. Inst. Div. of Atmos. Sci., Reno, Nev. [Available at http://www.atmospheric-research.com/PDFs/AuditSOPs/DRI%20Met%20Audit%20SOP.pdf.]

Desert Research Institute (DRI) (2002b), Performance audit of continuous ozone analyzers, *DRI SOP #4-101.2*, Desert Res. Inst. Div. of Atmos. Sci., Reno, Nev. [Available at http://www.atmospheric-research.com/PDFs/AuditSOPs/DRI%20Ozone%20Audit%20SOP.pdf.]

Desert Research Institute (DRI) (2002c), Performance audit of continuous gas analyzers, *DRI SOP #4-101.3*, Desert Res. Inst. Div. of Atmos. Sci., Reno, Nev. [Available at http://www.atmospheric-research.com/PDFs/AuditSOPs/DRI%20Trace%20Gas%20Audit%20SOP.pdf.]

Desert Research Institute (DRI) (2002d), Performance audit of Rupprecht and Patashnick Tapered Element Oscillating Microbalance (TEOM), *DRI SOP # 4-111.1*, Desert Res. Inst. Div. of Atmos. Sci., Reno, Nev. [Available at http://www.atmospheric-research.com/PDFs/AuditSOPs/DRI%20TEOM%20Audit%20SOP.pdf.]

Desert Research Institute (DRI) (2002e), Performance audit of continuous particulate sulfate, nitrate, and ammonium samplers, *DRI SOP # 4-116.1*, Desert Res. Inst. Div. of Atmos. Sci., Reno, Nev. [Available at http://www.atmospheric-research.com/PDFs/AuditSOPs/DRI%20SO4-NO3-NH4%20Audit%20SOP.pdf.]

Desert Research Institute (DRI) (2002f), Performance audit of Rupprecht and Patashnick carbon analyzer, Model 5400, *DRI SOP #4-110.1*, Desert Res. Inst. Div. of Atmos. Sci., Reno, Nev. [Available at http://www.atmospheric-research.com/PDFs/AuditSOPs/DRI%20Carbon%20Audit%20SOP.pdf.]

Edwards, D. P., et al. (2004), Observations of carbon monoxide and aerosols from the Terra satellite: Northern Hemisphere variability, *J. Geophys. Res.*, *109*, D24202, doi:10.1029/2004JD004727.

Ek, M. B., K. B. Mitchell, Y. Lin, B. Rogers, P. Grunmann, V. Koren, G. Gayno, and J. D. Tarpley (2003), Implementation of NOAH land surface model advances in the National Centers for Environmental Prediction

operational mesoscale Eta model, *J. Geophys. Res.*, *108*(D22), 8851, doi:10.1029/2002JD003296.

Emmerson, K. M., and M. J. Evans (2009), Comparison of tropospheric gas-phase chemistry schemes for use within global models, *Atmos. Chem. Phys.*, *9*, 1831–1845, doi:10.5194/acp-9-1831-2009.

Emmons, L. K., G. G. Pfister, D. P. Edwards, J. C. Gille, G. Sachse, D. Blake, S. Wofsy, C. Gerbig, D. Matross, and P. Nédélec (2007), Measurements of Pollution in the Troposphere (MOPITT) validation exercises during summer 2004 field campaigns over North America, *J. Geophys. Res.*, *112*, D12S02, doi:10.1029/2006JD007833.

Fahey, K. M., and S. N. Pandis (2001), Optimizing model performance: Variable size resolution in cloud chemistry modeling, *Atmos. Environ.*, *35*, 4471–4478, doi:10.1016/S1352-2310(01)00224-2.

Faraji, M., Y. Kimura, E. McDonald-Buller, and D. Allen (2008), Comparison of the carbon bond and SAPRC photochemical mechanisms under conditions relevant to southeast Texas, *Atmos. Environ.*, *42*, 5821–5836, doi:10.1016/j.atmosenv.2007.07.048.

Fast, J. D., W. I. Gustafson Jr., R. C. Easter, R. A. Zaveri, J. C. Barnard, E. G. Chapman, G. A. Grell, and S. E. Peckham (2006), Evolution of ozone, particulates, and aerosol direct radiative forcing on the vicinity of Houston using a fully coupled meteorology-chemistry-aerosol model, *J. Geophys. Res.*, *111*, D21305, doi:10.1029/2005JD006721.

Gao, B.-C., and Y. J. Kaufman (2003), Water vapor retrievals using Moderate Resolution Imaging Spectroradiometer (MODIS) near-infrared channels, *J. Geophys. Res.*, *108*(D13), 4389, doi:10.1029/2002JD003023.

Gery, M. W., G. Z. Whitten, J. P. Killus, and M. C. Dodge (1989), A photochemical kinetics mechanism for urban and regional scale computer modeling, *J. Geophys. Res.*, *94*(D10), 12,925–12,956, doi:10.1029/JD094iD10p12925.

Ghan, S. J., L. R. Leung, R. C. Easter, and H. Abdul-Razzak (1997), Prediction of cloud droplet number in a general circulation model, *J. Geophys. Res.*, *102*(D18), 21,777–21,794, doi:10.1029/97JD01810.

Gong, S. L., L. A. Barrie, and M. Lazare (2002), Canadian Aerosol Module (CAM): A size-segregated simulation of atmospheric aerosol processes for climate and air quality models: 2. Global sea-salt aerosol and its budgets, *J. Geophys. Res.*, *107*(D24), 4779, doi:10.1029/2001JD002004.

Grell, G. A., and D. Devenyi (2002), A generalized approach to parameterizing convection combining ensemble and data assimilation techniques, *Geophys. Res. Lett.*, *29*(14), 1693, doi:10.1029/2002GL015311.

Grell, G. A., S. Emeis, W. R. Stockwell, T. Schoenemeyer, R. Forkel, J. Michalakes, R. Knoche, and W. Seidl (2000), Application of a multiscale, coupled MM5/chemistry model to the complex terrain of the VOTALP valley campaign, *Atmos. Environ.*, *34*, 1435–1453, doi:10.1016/S1352-2310(99)00402-1.

Grell, G. A., S. E. Peckham, R. Schmitz, S. A. McKeen, G. Frost, W. C. Skamarock, and B. Eder (2005), Fully coupled "online" chemistry within the WRF model, *Atmos. Environ.*, *39*, 6957–6975, doi:10.1016/j.atmosenv.2005.04.027.

Gross, A., and W. R. Stockwell (2003), Comparison of the EMEP, RADM2 and RACM mechanisms, *J. Atmos. Chem.*, *44*, 151–170, doi:10.1023/A:1022483412112.

Gustafson, W. I., Jr., E. G. Chapman, S. J. Ghan, R. C. Easter, and J. D. Fast (2007), Impact on modeled cloud characteristics due to simplified treatment of uniform cloud condensation nuclei during NEAQS 2004, *Geophys. Res. Lett.*, *34*, L19809, doi:10.1029/2007GL030021.

Hansen, D. A., E. S. Edgerton, B. E. Hartsell, J. J. Jansen, N. Kandasamy, G. M. Hidy, and C. L. Blanchard (2003), The southeastern aerosol research and characterization study: Part 1. Overview, *J. Air Waste Manage. Assoc.*, *53*, 1460–1471.

Hong, S., Y. Noh, and J. Dudhia (2006), A new vertical diffusion package with an explicit treatment of entrainment processes, *Mon. Weather Rev.*, *134*, 2318–2341, doi:10.1175/MWR3199.1.

Hough, A. M. (1988), An intercomparison of mechanisms for the production of photochemical oxidants, *J. Geophys. Res.*, *93*(D4), 3789–3812, doi:10.1029/JD093iD04p03789.

Hyer, E. J., J. S. Reid, and J. Zhang (2010), An over-land aerosol optical depth data set for data assimilation by filtering, correction, and aggregation of MODIS Collection 5 optical depth retrievals, *Atmos. Meas. Tech. Discuss.*, *3*, 4091–4167, doi:10.5194/amtd-3-4091-2010.

Jacobson, M. Z. (2005), A solution to the problem of nonequilibrium acid/base gas-particle transfer at long time step, *Aerosol Sci. Technol.*, *39*, 92–103, doi:10.1080/027868290904546.

Jacobson, M. Z., R. P. Turco, E. J. Jensen, and O. B. Toon (1994), Modeling coagulation among particles of different composition and size, *Atmos. Environ.*, *28*, 1327–1338, doi:10.1016/1352-2310(94)90280-1.

Janjić, Z. I. (2001), *Nonsingular Implementation of the Mellor–Yamada Level 2.5 Scheme in the NCEP Meso Model, NCEP Off. Note 437*, 61 pp., Natl. Cent. for Environ. Predict., Camp Springs, Md.

Janssen, R. H. H., L. N. Ganzeveld, P. Kabat, M. Kulmala, T. Nieminen, and R. A. Roebeling (2011), Estimating seasonal variations in cloud droplet number concentration over the boreal forest from satellite observations, *Atmos. Chem. Phys.*, *11*, 7701–7713, doi:10.5194/acp-11-7701-2011.

Jimenez, P., J. M. Baldasano, and D. Dabdub (2003), Comparison of photochemical mechanisms for air quality modeling, *Atmos. Environ.*, *37*, 4179–4194, doi:10.1016/S1352-2310(03)00567-3.

Kanakidou, M., et al. (2005), Organic aerosol and global climate modeling: A review, *Atmos. Chem. Phys.*, *5*, 1053–1123, doi:10.5194/acp-5-1053-2005.

Karamchandani, P., Y. Zhang, S.-Y. Chen, and R. Balmori-Bronson (2011), Development of an extended chemical mechanism for global-through-urban applications, *Atmos. Pollut. Res.*, doi:10.5094/APR.2011.047, in press.

Kim, Y., K. Sartelet, and C. Seigneur (2009), Comparison of two gas-phase chemical kinetic mechanisms of ozone formation over Europe, *J. Atmos. Chem.*, *62*, 89–119, doi:10.1007/s10874-009-9142-5.

Kim, Y., K. Sartelet, and C. Seigneur (2011a), Formation of secondary aerosols: impact of the gas-phase chemical mechanism, *Atmos. Chem. Phys.*, *11*, 583–598, doi:10.5194/acp-11-583-2011.

Kim, Y., F. Couvidat, K. Sartelet, and C. Seigneur (2011b), Comparison of different gas-phase mechanisms and aerosol modules for simulating particulate matter formation, *J. Air Waste Manage. Assoc.*, *61*, 1218–1226, doi:10.1080/10473289.2011.603999.

Kuhn, M., et al. (1998), Intercomparison of the gas-phase chemistry in several chemistry and transport models, *Atmos. Environ.*, *32*, 693–709, doi:10.1016/S1352-2310(97)00329-4.

Li, Z., and A. P. Trishchenko (2001), Quantifying uncertainties in determining SW cloud radiative forcing and cloud absorption due to variability in atmospheric conditions, *J. Atmos. Sci.*, *58*, 376–389, doi:10.1175/1520-0469(2001)058<0376:QUIDSC>2.0.CO;2.

Liang, J., B. Jackson, and A. Kaduwela (2006), Evaluation of the ability of indicator species ratios to determine the sensitivity of ozone to reductions in emissions of volatile organic compounds and oxides of nitrogen in northern California, *Atmos. Environ.*, *40*, 5156–5166, doi:10.1016/j.atmosenv.2006.03.060.

Liebmann, B., and C. A. Smith (1996), Description of a complete (interpolated) outgoing longwave radiation dataset, *Bull. Am. Meteorol. Soc.*, *77*, 1275–1277.

Lin, Y.-L., R. D. Farley, and H. D. Orville (1983), Bulk parameterization of the snow field in a cloud model, *J. Clim. Appl. Meteorol.*, *22*, 1065–1092, doi:10.1175/1520-0450(1983)022<1065:BPOTSF>2.0.CO;2.

Liu, P., and Y. Zhang (2011), Use of a process analysis tool for diagnostic study on fine particulate matter predictions in the U.S. Part I: Model evaluation using surface, aircraft, and satellite data, *Atmos. Pollut. Res.*, *2*(1), 49–60, doi:10.5094/APR.2011.007.

Liu, Y., P. H. Daum, and R. L. McGraw (2005), Size truncation effect, threshold behavior, and a new type of autoconversion parameterization, *Geophys. Res. Lett.*, *32*, L11811, doi:10.1029/2005GL022636.

Lu, C.-H., and J. S. Chang (1998), On the indicator-based approach to assess ozone sensitivities and emissions features, *J. Geophys. Res.*, *103*, 3453–3462, doi:10.1029/97JD03128.

Luecken, D. J., S. Phillips, G. Sarwar, and C. Jang (2008), Effects of using the CB05 vs. SAPRC99 vs. CB4 chemical mechanism on model predictions: Ozone and gas-phase photochemical precursor concentrations, *Atmos. Environ.*, *42*, 5805–5820, doi:10.1016/j.atmosenv.2007.08.056.

McMurry, P. H., and S. K. Friedlander (1979), New particle formation in the presence of an aerosol, *Atmos. Environ.*, *13*, 1635–1651, doi:10.1016/0004-6981(79)90322-6.

McPeters, R. D., et al. (1998), *Earth Probe Total Ozone Mapping Spectrometer (TOMS) Data Products User's Guide, NASA Tech. Publ. 1998–206895*, 64 pp., NASA Goddard Space Flight Cent., Greenbelt, Md. [Available at http://cedadocs.badc.rl.ac.uk/107/1/earthprobe_userguide.pdf.].

Miao, J.-F., D. Chen, K. Wyser, K. Borne, J. Lindgren, M. K. S. Strandevall, S. Thorsson, C. Achberger, and E. Almkvist (2008), Evaluation of MM5 mesoscale model at local scale for air quality applications over the Swedish west coast: Influence of PBL and LSM parameterizations, *Meteorol. Atmos. Phys.*, *99*, 77–103, doi:10.1007/s00703-007-0267-2.

Milford, J. B., D. Gao, S. Sillman, P. Blossey, and A. G. Russell (1994), Total reactive nitrogen (NO_y) as an indicator of the sensitivity of ozone to reductions in hydrocarbon and NO_x emissions, *J. Geophys. Res.*, *99*(D2), 3533–3542, doi:10.1029/93JD03224.

Minvielle, F., et al. (2004), Modelling the transport of aerosols during INDOEX 1999 and comparison with experimental data. Part 2: Continental aerosols and their optical depth, *Atmos. Environ.*, *38*, 1823–1837, doi:10.1016/j.atmosenv.2003.12.033.

Mlawer, E. J., S. J. Taubman, P. D. Brown, M. J. Iacono, and S. A. Clough (1997), Radiative transfer for inhomogeneous atmospheres: RRTM, a validated correlated-k model for the longwave, *J. Geophys. Res.*, *102* (D14), 16,663–16,682, doi:10.1029/97JD00237.

Monin, A. S., and A. M. Obukhov (1954), Basic laws of turbulent mixing in the surface layer of the atmosphere [in Russian], *Tr. Geophiz. Inst. Akad. Nauk. SSSR*, *24*(151), 163–187.

Office of Air Quality Planning and Standards (OAQPS) (1999), *Quality Assurance Project Plan: $PM_{2.5}$ Speciation Trends Network Field Sampling (Final Draft)*, U.S. Environ. Prot. Agency, Research Triangle Park, N. C.

Office of Air Quality Planning and Standards (OAQPS) (2000), *Quality Assurance Guidance Document, Rep. EPA-454/R-01-001*, U.S. Environ. Prot. Agency, Research Triangle Park, N. C.

Office of Air Quality Planning and Standards (OAQPS) (2002), *IMPROVE: Interagency Monitoring of Protected Visual Environments Quality Assurance Project Plan*, U.S. Environ. Prot. Agency, Research Triangle Park, N. C. [Available at http://vista.cira.colostate.edu/IMPROVE/Publications/QA_QC/IMPROVE_QAPP_R0.pdf.]

Office of Air Quality Planning and Standards (OAQPS) (2007), *Guidance on the Use of Models and Other Analyses for Demonstrating Attainment of Air Quality Goals for Ozone, $PM_{2.5}$, and Regional Haze, Rep. EPA-454/B-07-002*, U.S. Environ. Prot. Agency, Research Triangle Park, N. C. [Available at http://www.epa.gov/scram001/guidance/guide/final-03-pm-rh-guidance.pdf.]

Office of Air Quality Planning and Standards (OAQPS) (2008), *Quality Assurance Handbook for Air Pollution Measurement Systems, Vol. II: Ambient Air Quality Monitoring Program, Rep. EPA-454/B-08-003*, U.S. Environ. Prot. Agency, Research Triangle Park, N. C. [Available at http://www.epa.gov/ttn/amtic/files/ambient/pm25/qa/QA-Handbook-Vol-II.pdf.]

Olson, J., et al. (1997), Results from the Intergovernmental Panel on Climate Change Photochemical Model Intercomparison (PhotoComp), *J. Geophys. Res.*, *102*(D5), 5979–5991, doi:10.1029/96JD03380.

Otkin, J. A., and T. J. Greenwald (2008), Comparison of WRF model-simulated and MODIS-derived cloud data, *Mon. Weather Rev.*, *136*, 1957–1970, doi:10.1175/2007MWR2293.1.

Otte, T. L. (2008a), The impact of nudging in the meteorological model for retrospective air quality simulations. Part II: Evaluating collocated meteorological and air quality observations, *J. Appl. Meteorol. Climatol.*, *47*, 1868–1887, doi:10.1175/2007JAMC1791.1.

Otte, T. L. (2008b), The impact of nudging in the meteorological model for retrospective air quality simulations. Part I: Evaluation against national observational networks, *J. Appl. Meteorol. Climatol.*, *47*, 1853–1867, doi:10.1175/2007JAMC1790.1.

Pincus, R., S. Platnick, S. A. Ackerman, R. S. Hemler, and R. J. P. Hofmann (2011), Reconciling simulated and observed views of clouds: MODIS, ISCCP, and the limits of instrument simulators, *J. Clim.*, in press.

Pun, B. K., C. Seigneur, J. Pankow, E. Chang, R. Griffin, and E. Knipping (2005), An upgraded absorptive secondary organic aerosol partitioning module for three-dimensional air quality applications, paper presented at the Twenty-Fourth Annual AAAR Conference, Austin, Tex., 17–21 October.

Remer, L. A., et al. (2005), The MODIS aerosol algorithm, products, and validation, *J. Atmos. Sci.*, *62*, 947–973, doi:10.1175/JAS3385.1.

Roy, B., R. Mathur, A. B. Gilliland, and S. C. Howard (2007), A comparison of CMAQ-based aerosol properties with IMPROVE, MODIS, and AERONET data, *J. Geophys. Res.*, *112*, D14301, doi:10.1029/2006JD008085.

Salzmann, M. (2007), Using KPP generated chemistry solvers in WRF-Chem, presented at the Eighth WRF Users' Workshop, Boulder, Colo., 11–15 June.

Salzmann, M. (2008), *WRF-Chem/KPP Coupler (WKC) for WRF V3, Users' and Developers Guide v2.0*, Princeton Univ. Press, Princeton, N. J.

Sanjay, J. (2008), Assessment of atmospheric boundary-layer processes represented in the numerical model MM5 for a clear sky day using LASPEX observations, *Boundary Layer Meteorol.*, *129*, 159–177, doi:10.1007/s10546-008-9298-6.

Sarwar, G., D. Luecken, G. Yarwood, G. Z. Whitten, and W. P. L. Carter (2008), Impact of an updated carbon bond mechanism and predictions from the CMAQ modeling system: Preliminary assessment, *J. Appl. Meteorol. Climatol.*, *47*, 3–14, doi:10.1175/2007JAMC1393.1.

Sarwar, G., K. W. Appel, A. G. Carlton, R. Mathur, K. Schere, R. Zhang, and M. Majeed (2011), Impact of a new condensed toluene mechanism on air quality model predictions in the US, *Geosci. Model Dev.*, *4*, 183–193, doi:10.5194/gmd-4-183-2011.

Seethala, C. (2011), Cloud liquid water path from spaceborne measurements, paper presented at Climate Observation Science Meeting, KNMI, De Bilt, Netherlands, 17 January.

Seinfeld, J. H., and J. F. Pankow (2003), Organic atmospheric particulate material, *Annu. Rev. Phys. Chem.*, *54*, 121–140, doi:10.1146/annurev.physchem.54.011002.103756.

Sillman, S. (1995), The use of NO_y, H_2O_2, and HNO_3 as indicators for ozone-NO_x-hydrocarbon sensitivity in urban locations, *J. Geophys. Res.*, *100*(D7), 14,175–14,188, doi:10.1029/94JD02953.

Sillman, S., D. He, C. Cardelino, and R. E. Imhoff (1997), The use of photochemical indicators to evaluate ozone-NO_x-hydrocarbon sensitivity: Case studies from Atlanta, New York, and Los Angeles, *J. Air Waste Manage. Assoc.*, *47*, 642–652.

Skamarock, W. C., and M. L. Weisman (2009), The impact of positive-definite moisture transport on NWP precipitation forecasts, *Mon. Weather Rev.*, *137*, 488–494, doi:10.1175/2008MWR2583.1.

Skamarock, W. C., J. B. Klemp, J. Dudhia, D. O. Gill, D. M. Barker, W. Wang, and J. G. Powers (2005), *A Description of the Advanced Research WRF Version 2, Tech. Note NCAR/TN-468+STR*, 88 pp., Natl. Cent. for Atmos. Res., Boulder, Colo. [Available at http://wrf-model.org/wrfadmin/publications.php.].

Southeastern Aerosol Research and Characterization Study (SEARCH) (2003), Search methodology for construction of pie and bar charts using $PM_{2.5}$ speciation data, SEARCH data and metric protocols, Atmos. Res. and Anal., Inc., Plano, Tex. [Available at http://www.atmospheric-research.com/method/index.html.]

Tarasova, T. A., J. P. R. Fernandez, I. A. Pisnichenko, J. A. Marengo, J. C. Ceballos, and M. J. Bottino (2006), Impact of new solar radiation parameterization in the Eta model on the simulation of summer climate over South America, *J. Appl. Meteorol. Climatol.*, *45*, 318–333, doi:10.1175/JAM2342.1.

Tonnesen, G. S., and R. L. Dennis (2000a), Analysis of radical propagation efficiency to assess ozone sensitivity to hydrocarbons and NO_x 1. Local indicators of instantaneous odd oxygen production sensitivity, *J. Geophys. Res.*, *105*(D7), 9213–9225, doi:10.1029/1999JD900371.

Tonnesen, G. S., and R. L. Dennis (2000b), Analysis of radical propagation efficiency to assess ozone sensitivity to hydrocarbons and NO_x 2. Long-lived species as indicators of ozone concentration sensitivity, *J. Geophys. Res.*, *105*(D7), 9227–9241, doi:10.1029/1999JD900372.

Turpin, B. J., and H. J. Lim (2001), Species contributions to $PM_{2.5}$ mass concentrations: revisiting common assumptions for estimating organic mass, *Aerosol Sci. Technol.*, *35*, 602–610.

U.S. Environmental Protection Agency (EPA) (1983), *Quality Assurance Handbook for Air Pollution Measurement Systems: Volume 5. Manual for Precipitation Measurement Systems, Rep. EPA-600/4-82-042a&b*, U.S. Environ. Prot. Agency, Research Triangle Park, N. C. [Available at http://nepis.epa.gov/EPA/html/Pubs/pubalpha_Q.html.]

White, W. H., and P. T. Roberts (1977), On the nature and origins of visibility-reducing aerosols in the Los Angeles air basin, *Atmos. Environ.*, *11*, 803–812, doi:10.1016/0004-6981(77)90042-7.

Whitten, G. Z., G. Heo, Y. Kimura, E. McDonald-Buller, D. T. Allen, W. P. L. Carter, and G. Yarwood (2010), A new condensed toluene mechanism for Carbon Bond: CB05-TU, *Atmos. Environ.*, *44*, 5346–5355, doi:10.1016/j.atmosenv.2009.12.029.

Wild, O., X. Zhu, and M. J. Prather (2000), Fast-J: Accurate simulation of in- and below-cloud photolysis in tropospheric chemical models, *J. Atmos. Chem.*, *37*, 245–282, doi:10.1023/A:1006415919030.

Xie, P., and P. A. Arkin (1997), Global precipitation: A 17-year monthly analysis based on gauge observations, satellite estimates, and numerical model outputs, *Bull. Am. Meteorol. Soc.*, *78*, 2539–2558, doi:10.1175/1520-0477(1997)078<2539:GPAYMA>2.0.CO;2.

Yarwood, G., T. E. Stoeckenius, J. G. Heiken, and A. M. Dunker (2003), Modeling weekday/weekend ozone differences in the Los Angeles region for 1997, *J. Air Waste Manag. Assoc.*, *53*, 864–875.

Yarwood, G., S. Rao, M. Yocke, and G. Z. Whitten (2005), *Final Report—Updates to the Carbon Bond Chemical Mechanism: CB05, Rep. RT-04-00675*, 246 pp., Yocke and Co., Novato, Calif. [Available at http://www.camx.com/publ/pdfs/CB05_Final_Report_120805.pdf.].

Yu, S., R. Mathur, K. Schere, D. Kang, J. Pleim, J. Young, D. Tong, G. Pouliot, S. A. McKeen, and S. T. Rao (2008), Evaluation of real-time $PM_{2.5}$ forecasts and process analysis for $PM_{2.5}$ formation over the eastern United States using the Eta-CMAQ forecast model during the 2004 ICARTT Study, *J. Geophys. Res.*, *113*, D06204, doi:10.1029/2007JD009226.

Zaveri, R. A., and L. K. Peters (1999), A new lumped structure photochemical mechanism for large-scale applications, *J. Geophys. Res.*, *104*(D23), 30,387–30,415, doi:10.1029/1999JD900876.

Zhang, N., Y.-S. Chen, and Y. Zhang (2011), Forecasting O_3 and $PM_{2.5}$ during summer and winter with WRF/Chem-MADRID over the southeastern United States, poster presented at the Tenth Annual CMAS Conference, Chapel Hill, N. C., 24–26 October.

Zhang, Y. (2008), Online coupled meteorology and chemistry models: History, current status, and outlook, *Atmos. Chem. Phys.*, *8*, 2895–2932, doi:10.5194/acp-8-2895-2008.

Zhang, Y., B. Pun, K. Vihayaraghavan, S.-Y. Wu, C. Seigneur, S. N. Pandis, M. Z. Jacobson, A. Nenes, and J. H. Seinfeld (2004), Development and application of the Model of Aerosol Dynamics, Reaction, Ionization, and Dissolution (MADRID), *J. Geophys. Res.*, *109*, D01202, doi:10.1029/2003JD003501.

Zhang, Y., P. Liu, B. Pun, and C. Seigneur (2006a), A comprehensive performance evaluation of MM5-CMAQ for summer 1999 Southern Oxidants Study Episode, Part I. Evaluation protocols, databases, and meteorological predictions, *Atmos. Environ.*, *40*, 4825–4838, doi:10.1016/j.atmosenv.2005.12.043.

Zhang, Y., P. Liu, B. Pun, and C. Seigneur (2006b), A comprehensive performance evaluation of MM5-CMAQ for the summer 1999 Southern Oxidants Study Episode, Part III. Diagnostic and mechanistic evaluations, *Atmos. Environ.*, *40*, 4856–4873, doi:10.1016/j.atmosenv.2005.12.046.

Zhang, Y., X.-Y. Wen, K. Wang, K. Vijayaraghavan, and M. Z. Jacobson (2009), Probing into regional O_3 and PM pollution in the U.S., Part II. An examination of formation mechanisms through a process analysis technique and sensitivity study, *J. Geophys. Res.*, *114*, D22305, doi:10.1029/2009JD011900.

Zhang, Y., Y. Pan, K. Wang, J. D. Fast, and G. A. Grell (2010a), WRF/Chem-MADRID: Incorporation of an aerosol module into WRF/Chem and its initial application to the TexAQS2000 episode, *J. Geophys. Res.*, *115*, D18202, doi:10.1029/2009JD013443.

Zhang, Y., X.-Y. Wen, and C. J. Jang (2010b), Simulating chemistry–aerosol–cloud–radiation–climate feedbacks over the continental U.S. using the online-coupled Weather Research Forecasting Model with chemistry (WRF/Chem), *Atmos. Environ.*, *44*, 3568–3582, doi:10.1016/j.atmosenv.2010.05.056.

Zhang, Y., P. Liu, X.-H. Liu, B. Pun, C. Seigneur, M. Z. Jacobson, and W.-X. Wang (2010c), Fine scale modeling of wintertime aerosol mass, number, and size distributions in central California, *J. Geophys. Res.*, *115*, D15207, doi:10.1029/2009JD012950.

Zhang, Y., Y.-S. Chen, S.-Y. Wu, S. Zhu, K. Sartelet, P. Tran, and C. Seigneur (2011), Application of WRF/Chem-MADRID in Europe: Model evaluation and aerosol-meteorology interactions, paper presented at the European Geosciences Union General Assembly 2011, Vienna, Austria, 3–8 April.

Zhu, S., and Y. Zhang (2011), Sensitivity of simulated chemical concentrations and aerosol-meteorology interactions to aerosol treatments in WRF/Chem, paper presented at the COST Action ES1004: "EuMetChem" scientific meeting, Vienna, Austria, 3–8 April.

Y. Chen and Y. Zhang, Department of Marine, Earth, and Atmospheric Sciences, North Carolina State University, Campus Box 8208, Raleigh, NC 27695, USA. (yang_zhang@ncsu.edu)

G. Sarwar and K. Schere, Atmospheric Modeling and Analysis Division, National Exposure Research Laboratory, U.S. Environmental Protection Agency, Research Triangle Park, NC 27711, USA.